Article

Cell Reports

RGS6 Mediates Effects of Voluntary Running on Adult Hippocampal Neurogenesis

Graphical Abstract

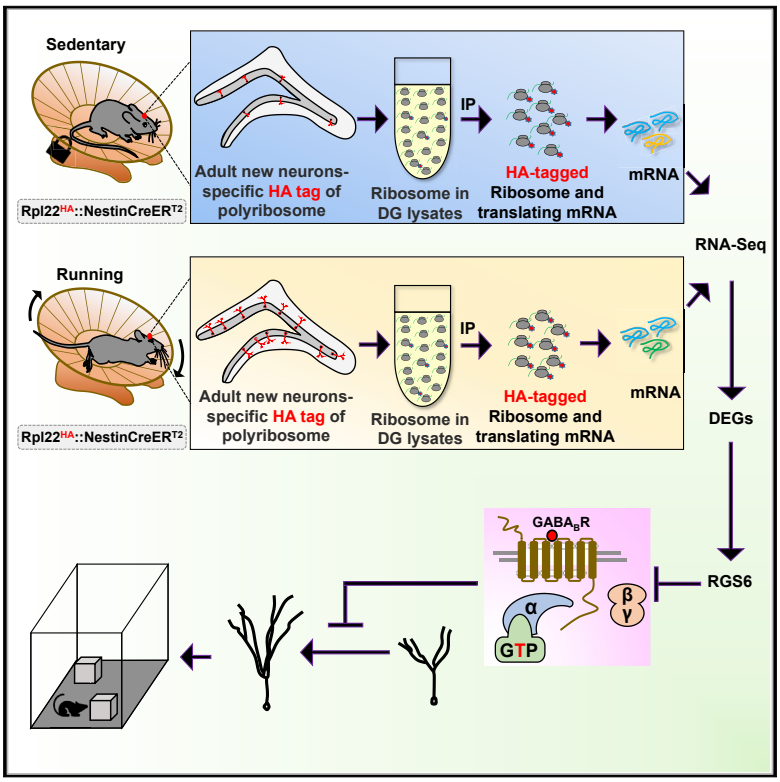

Highlights

- Adult new neurons display unique translational responses to voluntary running
- RGS6 increase in adult-born neurons mimics running effects on adult neurogenesis
- RGS6 increase reduces the inhibitory effect of $GABA_B$ receptor on adult neurogenesis
- RGS6 knockdown abolishes the running effect on adult neurogenesis and behaviors

Authors

Yu Gao, Minjie Shen, Jose Carlos Gonzalez, ..., Daifeng Wang, Linda Overstreet-Wadiche, Xinyu Zhao

Correspondence

xinyu.zhao@wisc.edu

In Brief

Gao et al. use translational profiling to unveil genome-wide intrinsic molecular changes in adult-born hippocampal neurons that contribute to voluntary running-enhanced adult neurogenesis. The molecular mediators identified, such as RGS6, are necessary for accelerated neuronal maturation and improved learning and memory in running mice.

Gao et al., 2020, Cell Reports *32*, 107997
August 4, 2020
https://doi.org/10.1016/j.celrep.2020.107997

CellPress

Cell Reports

CellPress
OPEN ACCESS

Article

RGS6 Mediates Effects of Voluntary Running on Adult Hippocampal Neurogenesis

Yu Gao,[1,2] Minjie Shen,[1,2] Jose Carlos Gonzalez,[3] Qiping Dong,[1] Sudharsan Kannan,[1,2] Johnson T. Hoang,[1,2] Brian E. Eisinger,[1,2] Jyotsna Pandey,[1] Sahar Javadi,[1] Qiang Chang,[1,4,5] Daifeng Wang,[1,6] Linda Overstreet-Wadiche,[3] and Xinyu Zhao[1,2,7,*]

[1]Waisman Center, University of Wisconsin-Madison, Madison, WI 53705, USA
[2]Department of Neuroscience, School of Medicine and Public Health, University of Wisconsin-Madison, Madison, WI 53705, USA
[3]Department of Neurobiology, University of Alabama at Birmingham, Birmingham, AL 35294, USA
[4]Department of Medical Genetics, School of Medicine and Public Health, University of Wisconsin-Madison, Madison, WI 53705, USA
[5]Department of Neurology, School of Medicine and Public Health, University of Wisconsin-Madison, Madison, WI 53705, USA
[6]Department of Biostatistics and Medical Informatics, School of Medicine and Public Health, University of Wisconsin-Madison, Madison, WI 53705, USA
[7]Lead Contact
*Correspondence: xinyu.zhao@wisc.edu
https://doi.org/10.1016/j.celrep.2020.107997

SUMMARY

Voluntary running enhances adult hippocampal neurogenesis, with consequences for hippocampal-dependent learning ability and mood regulation. However, the underlying mechanism remains unclear. Here, we show that voluntary running induces unique and dynamic gene expression changes specifically within the adult-born hippocampal neurons, with significant impact on genes involved in neuronal maturation and human diseases. We identify the regulator of G protein signaling 6 (RGS6) as a key factor that mediates running impact on adult-born neurons. RGS6 overexpression mimics the positive effects of voluntary running on morphological and physiological maturation of adult new neurons and reduced sensitivity of adult-born neurons to the inhibitory effect of $GABA_B$ (γ-Aminobutyric acid B) receptor activation. Knocking down RGS6 abolishes running-enhanced neuronal maturation and hippocampal neurogenesis-dependent learning and anxiolytic effect. Our study provides a data resource showing genome-wide intrinsic molecular changes in adult-born hippocampal neurons that contribute to voluntary running-induced neurogenesis.

INTRODUCTION

Adult mammalian neurogenesis persists at a low level in the dentate gyrus (DG), where radial glial-like neural stem cells (NSCs) give rise to immediate progenitors (IPCs) that subsequently differentiate into new DG neurons integrating into the hippocampal circuity (Kempermann et al., 2015). Although the extent of adult neurogenesis in humans remains unresolved, mounting evidence supports important roles of adult hippocampal neurogenesis in neuroplasticity, brain homeostasis, and behavioral adaptations (Deng et al., 2010; Hochgerner et al., 2018; Kempermann et al., 2015). Reduced adult hippocampal neurogenesis has been shown in neurodevelopmental and neurodegenerative diseases, as well as normal aging, which may contribute to decline in cognitive functions (Christian et al., 2014; Thompson et al., 2008; Winner and Winkler, 2015). Therefore, enhancing adult neurogenesis has been considered as a potential therapeutic method (Yun et al., 2016). Adult neurogenesis is sensitive to external stimuli and experiences (Aimone et al., 2010; Eisinger and Zhao, 2018). Among the positive stimuli, voluntary running is one of the most effective methods for promoting adult hippocampal neurogenesis. Since its first discovery (Kempermann et al., 1997; van Praag et al., 1999), extensive experimental evidence has supported that voluntary running significantly elevates adult hippocampal neurogenesis and improves hippocampus-dependent learning and memory (reviewed by Eisinger and Zhao, 2018; Vivar et al., 2013). At the cellular level, voluntary running promotes adult NSC activation (Dong et al., 2019), increases NSC and IPC proliferation (van Praag et al., 1999), elevates immature neuron survival (Snyder et al., 2009), accelerates morphological maturation (Eadie et al., 2005; Sah et al., 2017; Steib et al., 2014), and enhances integration of new neurons (Deshpande et al., 2013; Piatti et al., 2011; Trinchero et al., 2017; Vivar et al., 2016). In fact, voluntary running is one of the most effective methods for reversing the negative impact of aging and neurodegeneration on both adult neurogenesis and cognitive impairment (Berchtold et al., 2019; Trinchero et al., 2017). However, the mechanism underlying the effect of voluntary running on adult hippocampal neurogenesis remains poorly understood.

Both candidate gene approaches and more recently genome-wide transcriptomic methods have been used to interrogate the hippocampal or DG tissues of running animals, and several genes have been identified, for example, brain-derived neurotrophic factor (*Bdnf*) (reviewed by Eisinger and Zhao, 2018). Although exercise-activated C-FOS-positive cells have been

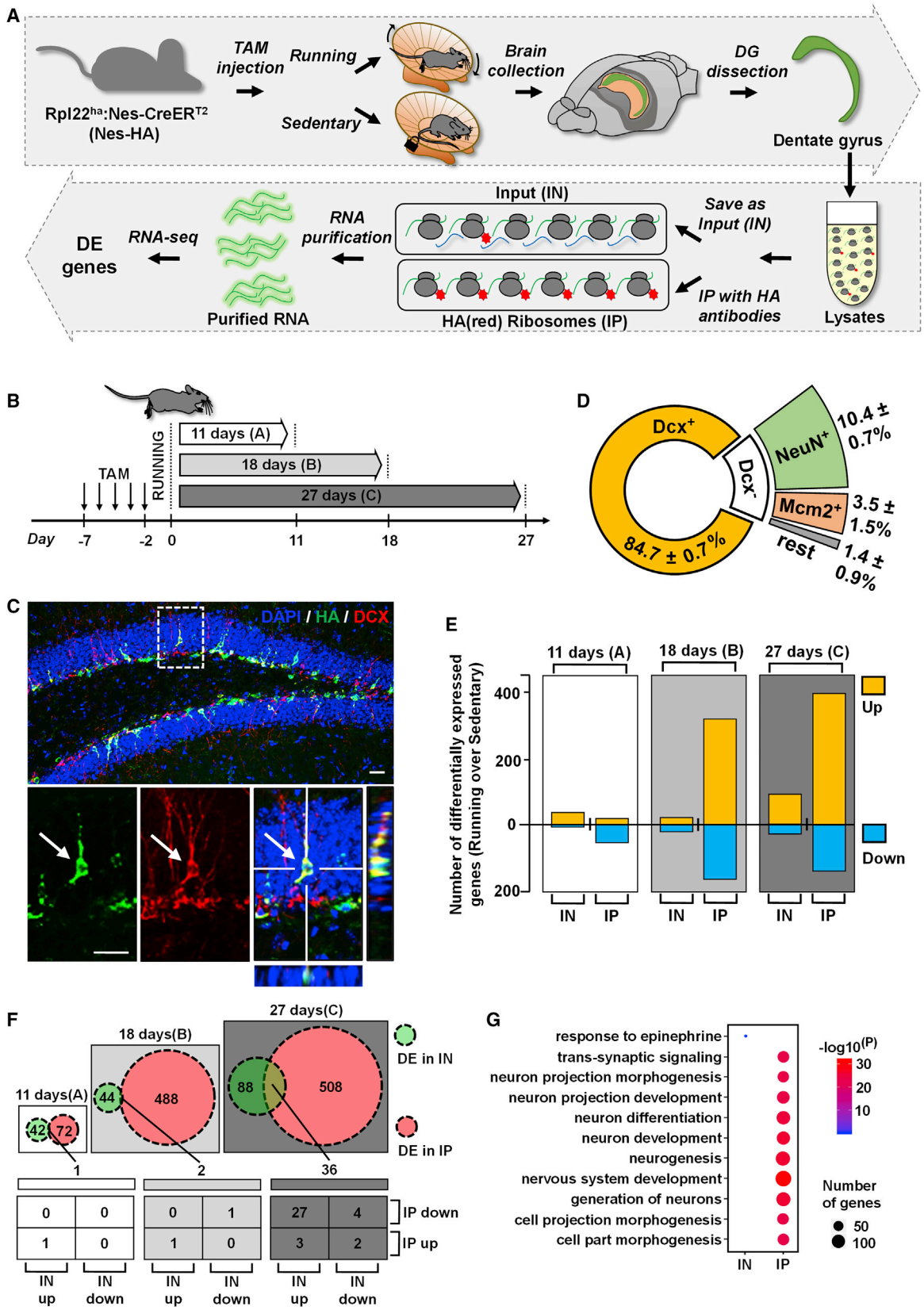

(legend on next page)

isolated for transcriptomic analysis (Chatzi et al., 2019), no study has illustrated genome-wide expression profiles within adult newborn neurons in response to voluntary running. Because adult new neurons constitute an extremely small portion of the entire cell population of the DG tissue that contains mostly mature neurons and glia, as well as many other cell types (Hochgerner et al., 2018), the differentially expressed genes (DEGs) identified in the hippocampal or DG tissues may not represent those DEGs in the new neurons. The small number of adult newborn neurons presents a major challenge for genome-wide assessment, specifically in these cells.

In this study, we showed that adult-born neurons mounted dynamic translational changes in response to voluntary running, with significant impact on genes involved in neuronal maturation and human diseases. We found that G protein signaling 6 (RGS6) is a key mediator of running-induced neurogenesis. Overexpression (OE) of RGS6 in adult new neurons increased morphological and electrophysiological maturation and reduced their sensitivity to the inhibitory effect of $GABA_B$ receptor activation, mimicking the effects of running. Knocking down RGS6 in adult new neurons abolished running-enhanced neuronal maturation and hippocampal neurogenesis-dependent learning and anxiolytic effect. Our study has provided a genome-wide view of intrinsic molecular changes in the adult newborn neurons and unveiled mechanisms underlying voluntary running-enhanced neurogenesis.

RESULTS

Adult-Born New Neurons Mount Unique and Dynamic Translational Responses to Voluntary Running

Voluntary running leads to increased cell proliferation in the subgranular zone (SGZ) of the DG (van Praag et al., 1999). To validate our running platform, we analyzed mice that have been running for 7 days and observed a significant increase (1.6-fold) in the number of bromodeoxyuridine (BrdU)-labeled cells in the running mice compared with controls (Figures S1A–S1C). A major challenge in studying gene expression in adult-born new DG neurons is the extremely small number of these new cells among vast mature cell populations. Fluorescent-activated cell sorting used by others (Bracko et al., 2012) and us (Gao et al., 2017) is disruptive to live cells (Lacar et al., 2016). We therefore chose a conditional ribosome tagging (RiboTag) technology by generating inducible adult new neuron-specific ribosome-tagging mice (*Rpl22^{HA}:Nes-CreER^{T2}*; termed Nes-HA) through crossing inducible *Nes-CreER^{T2}* driver mice and conditional ribosome tagging mice (Rpl22^{HA}) (Sanz et al., 2009). Tamoxifen (Tam) injection of Nes-HA mice leads to HA tagging of ribosomes specifically in NESTIN-expressing NSCs and their differentiated progenies (Figure 1A). To investigate translational responses to running in adult-born new neurons at different stages of neuronal development, we exposed the mice to wheels for three different time periods representing early, middle, and late stages of developmental maturation of adult new neurons (Kempermann et al., 2015): 11, 18, and 27 days (Figure 1B). We first assessed the specificity of ribosome tagging. As expected, nearly all HA^+ cells were located in the SGZ of the DG (Figure 1C; Figure S1). In both the 11- and 18-day sedentary mice, around 80% HA^+ cells expressed immature neuron marker Doublecortin (DCX; Figure 1D; Figures S1D–S1H). The percentage of DCX-positive (DCX^+) cells among HA^+ cells dropped to ~65%, but the percentage of HA^+ cells expressing mature neuron marker NeuN (Neuronal Nuclear Antigen, also known as Rbfox3) ($NeuN^+HA^+$) increased to ~80% in 27-day sedentary mice (Figures S1G and S1H), which is expected as a result of continuous maturation of HA^+ cells. In the 18-day sedentary mice, 84.7% ± 0.7% HA^+ cells were DCX^+, 10.4% ± 0.7% were DCX^-NeuN^+, 3.5% ± 1.5% were DCX^-MCM2^+ cells, and only 1.4% ± 0.9% were other cell types (Figures 1C and 1D). Thus, most of the HA^+DCX^- cells were either mature neurons or dividing progenitors. Similar cell fate results were obtained in HA^+ cells of running mice (Figures S1E–S1H). Therefore, Tam injection into Nes-HA mice leads to HA tagging ribosome (RiboTag) specifically in adult NSCs and their differentiated progenies in both running and sedentary mice, and the majority of cells labeled at all three time points were DCX^+ neurons undergoing neuronal maturation.

We dissected DG tissues from another cohort of mice to perform RiboTag immunoprecipitation (IP) of HA-tagged ribosomes together with their associated translating mRNAs. The IP mRNAs, as well as input (IN) mRNAs, were then identified by RNA sequencing (RiboTag-seq) (Figure 1A). There was no strong batch effect among both IP and IN samples (Figures S2A and S2B). We then performed PCA analysis of all 12 IP samples. The samples from 18- and 27-day, but not 11-day, running mice can be successfully separated from corresponding sedentary mice (Figure S2C). DEGs were successfully identified in running mice using embedded EBseq in RSEM (RNA-Seq by expectation maximization) with a cutoff of 0.05 of "PPEE" (posterior probability estimated by EBseq that a gene/transcript is equally expressed) (Table S1). *Bdnf* showed higher expression in the running mice compared with control sedentary mice in both IP and IN samples, whereas *Calb2* (Calretinin) showed higher expression in only IP samples (Figures S2D and S2E), consistent with the published literature (Brandt et al., 2003).

Overall, the IP samples (new neurons) had more DEGs than IN samples (DG tissue). Both IP and IN had more upregulated genes compared with downregulated genes in both the 18-day and the

Figure 1. Adult-Born Hippocampal Neurons Mount Unique and Dynamic Translational Responses to Voluntary Running

(A) A schematic drawing of the experimental design for translational profiling of adult new neurons in running and sedentary mice using RiboTag-seq.

(B) Experimental scheme for RiboTag-seq of mice subjected to running and sedentary treatments for three different time periods.

(C) Confocal images showing that most HA-positive (HA^+, green) cells are Doublecortin-positive (DCX^+, red) in 18-day sedentary mice. Scale bar, 50 μm.

(D) Pie chart depicting the percentages of DCX^+, $NeuN^+$, and $MCM2^+$ in HA^+ cells in 18-day sedentary mice. Data are presented as mean ± SEM.

(E) Bar chart depicting numbers of upregulated or downregulated genes in the IN and IP samples in running mice.

(F) Numbers of shared differentially expressed genes (DEGs) in the IN and IP samples in running mice.

(G) GO analysis (top biological process GO terms) of the unique DEGs in the IN and IP in 27-day samples (the "88 genes" [IN] and "508 genes" [IP] in F).

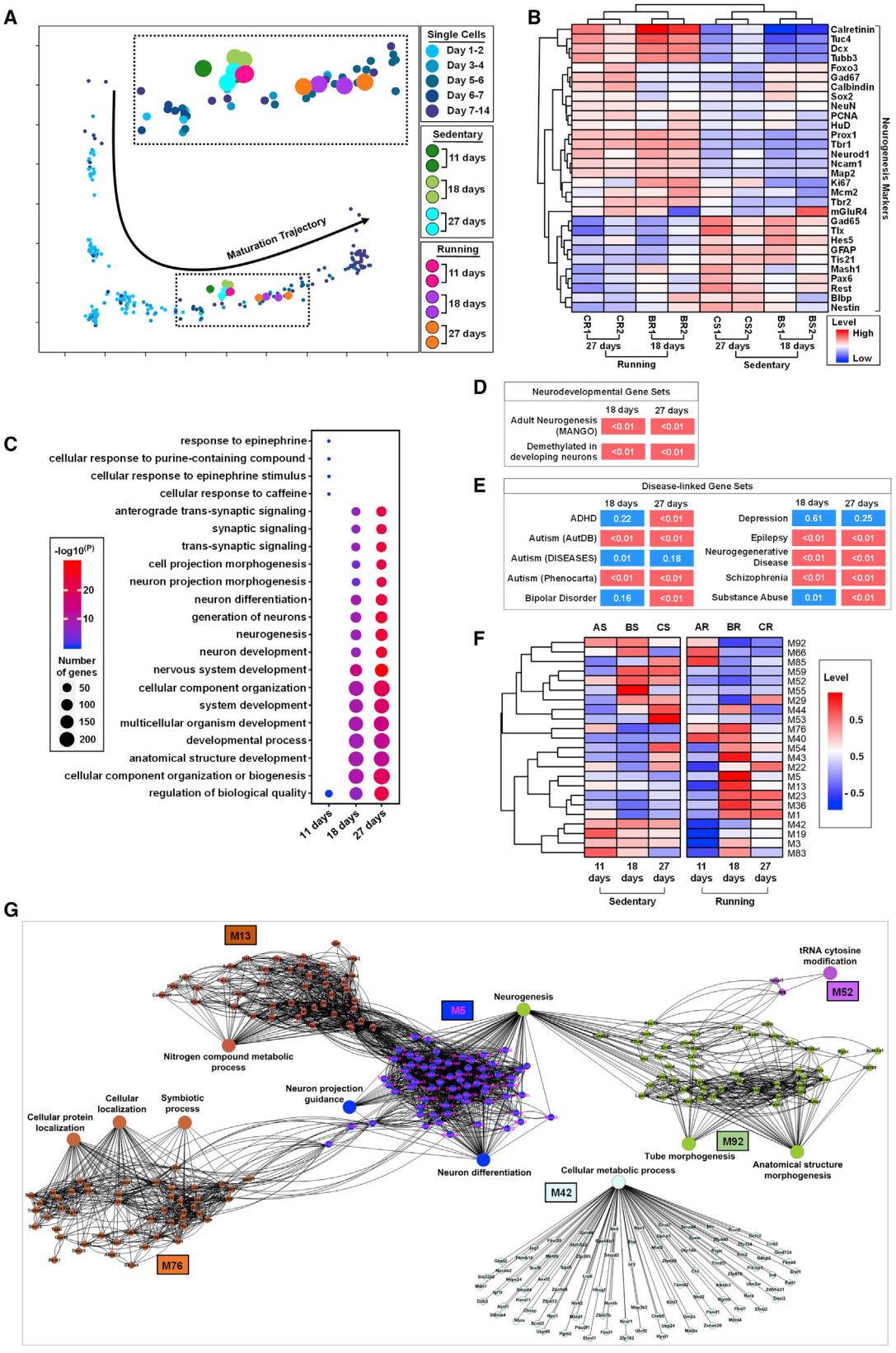

(legend on next page)

27-day time points (Figure 1E). Interestingly, there were only one and two DEGs shared between IP and IN samples at the 11- and 18-day time points, respectively. In contrast, 36 DEGs were shared between the IP and IN samples at the 27-day time point (Figure 1F; Table S1). Among the shared DEGs at 11 days, *Mylk3* (myosin light chain kinase 3) was upregulated in both IP and IN. Among the two shared DEGs at 18 days, *Ttr* (transthyretin) was upregulated in both IP and IN, whereas *Csmd3* (CUB and Sushi multiple domains 3) was downregulated in both IP and IN samples. To our surprise, in 27-day samples, 29 out of 36 DEGs showed opposite directions of changes in IN versus IP, with two genes upregulated in IP but downregulated in the IN and 27 genes downregulated in IP but upregulated in the IN (Figure 1F), suggesting that new neurons responded differently to running compared with other mature DG cells. We performed Gene Ontology (GO) analysis (Table S2) of the unique DEGs in IN (88 DEGs in Figure 1F) and IP (508 DEGs in Figure 1F) samples separately. The 88 genes DEGs in IN were associated with only one biological process GO term, "response to epinephrine cellular" (Figure 1G); in contrast, the 508 unique DEGs in IP were related to many neurogenesis and neuronal maturation-related biological process GO terms (Figure 1G). We also performed pathway analysis of the 29 DEGs that showed opposite directions in IP versus IN in 27-day samples and identified cytosolic calcium ion concentration as one of seven biological processes and membrane as the only cellular component, suggesting possible changes in neuronal activities in running mice (Table S2). In summary, these results demonstrate that adult-born new neurons mount distinct gene expression response to voluntary running compared with the majority of other cells residing in the DG.

Voluntary Running Leads to Dynamic Gene Expression Changes in Adult-Born New Neurons across Stages of Neurogenesis

Single-nuclei RNA sequencing has identified transcriptional signatures of adult new DG cells over a 14-day period post-BrdU labeling (Habib et al., 2016). To interrogate the neurogenic stages of our IP samples, we utilized the data from Habib et al. (2016) to create a developmental trajectory using pseudotime analysis by Monocle (Habib et al., 2016; Trapnell et al., 2014). Using DEGs between running and sedentary as transcriptional signatures, we recovered the developmental trajectory of adult-born DG neurons over 14 days (Habib et al., 2016) and mapped gene expression profiles of our IP samples onto this trajectory (Figure 2A). The sedentary samples and 11-day running samples were clustered together with immature cells on the trajectory, implying that neither the sedentary condition nor the short period running elicit significant impact on the neuronal maturation process. On the other hand, the 18- and 27-day running samples were separated from other samples and mapped to more mature neurons. This suggests that the effects of running appear after a longer period of voluntary running, and new neurons in running mice mature faster compared with those in the control sedentary mice.

To further validate this observation, we assessed the expression patterns of 30 genes that have been widely used to define the developmental stages of adult neurogenesis. Although there were fewer DEGs at the 11-day time point, running groups could be separated from the sedentary groups, with 18 neurogenesis early-stage-associated genes (Figure S2H), including striking upregulation of *Calb2* (Figures S2F and S2G), an immature neuron maker shown to be upregulated in response to running (Brandt et al., 2003; Grégoire et al., 2014). For the 18- and 27-day time points, running groups were clearly separated from the sedentary groups, and different time points were also separated from each other (Figure 2B). The genes corresponding to both immature neurons (e.g., *Calb2*, *Dcx*, *NeuroD1*, and *Tbr2*) and mature neurons (e.g., *HuD*, *Map2*, *Prox1*) exhibited higher translational levels in running groups compared with controls, whereas genes corresponding to immature NSCs and IPCs (*Nestin*, *Pax6*, and *Tlx*) displayed lower translational levels in the running group compared with controls.

We performed GO analysis of DEGs (Table S2) and compiled the top 10 biological process GO terms from each time point (Figure 2D). Interestingly, four out of the top five biology process GO terms in the 11-day running condition were specific to the 11-day condition, such as response to epinephrine (Figure 2C). On the other hand, both the 18- and 27-day running time points had top biological process GO terms related to neuronal differentiation and maturation-related neurogenesis processes (Figure 2C). In addition, the DEGs in the 18- and 27-day time points were significantly enriched with genes regulating adult hippocampal neurogenesis (MANGO; Overall et al., 2012) and genes exhibiting dynamic DNA demethylation in cortical neurons during post-natal neuronal maturation (Lister et al., 2013; Figure 2D). We have shown that genes upregulated in more mature DCX-expressing cells in the adult DG are significantly enriched for genes involved in autism-related disorders (Gao et al., 2017). Using a similar analysis, we found that the DEGs in both 18- and 27-day time points were significantly enriched for genes associated with both neurodevelopmental and neurodegenerative disorders, such as autism, schizophrenia,

Figure 2. Adult New Neurons Exhibit Dynamic Gene Expression Changes across Stages of Neurogenesis in Response to Running

(A) Mapping of IP samples from running and sedentary mice in neuronal maturation single-cell trajectory.

(B) Heatmap of 30 known neurogenesis-related markers in 18- and 27-day IP samples in sedentary and running mice.

(C) GO analysis of DEGs in 11-, 18-, and 27-day running mice.

(D) Enrichment of 18- and 27-day DEGs that are implicated in adult hippocampal neurogenesis and DNA demethylation in neurons during post-natal cortical development.

(E) Enrichment heatmap for disease-related genes in 18- and 27-day DEGs. Diseases are represented by rows, and DEGs are represented by columns. p values are shown in each cell and are color coded ($p < 0.01$ [red] and $p > 0.01$ or $p = 0.01$ [blue]). The Autism1 gene set was curated by Phenocarta, Autism2 by AutDB, and Autism3 by the DISEASES database. All other gene sets are from Phenocarta.

(F) Top 23 most different eigengene modules in sedentary and running mice.

(G) Gene network of the top 23 eigengene module genes in (F).

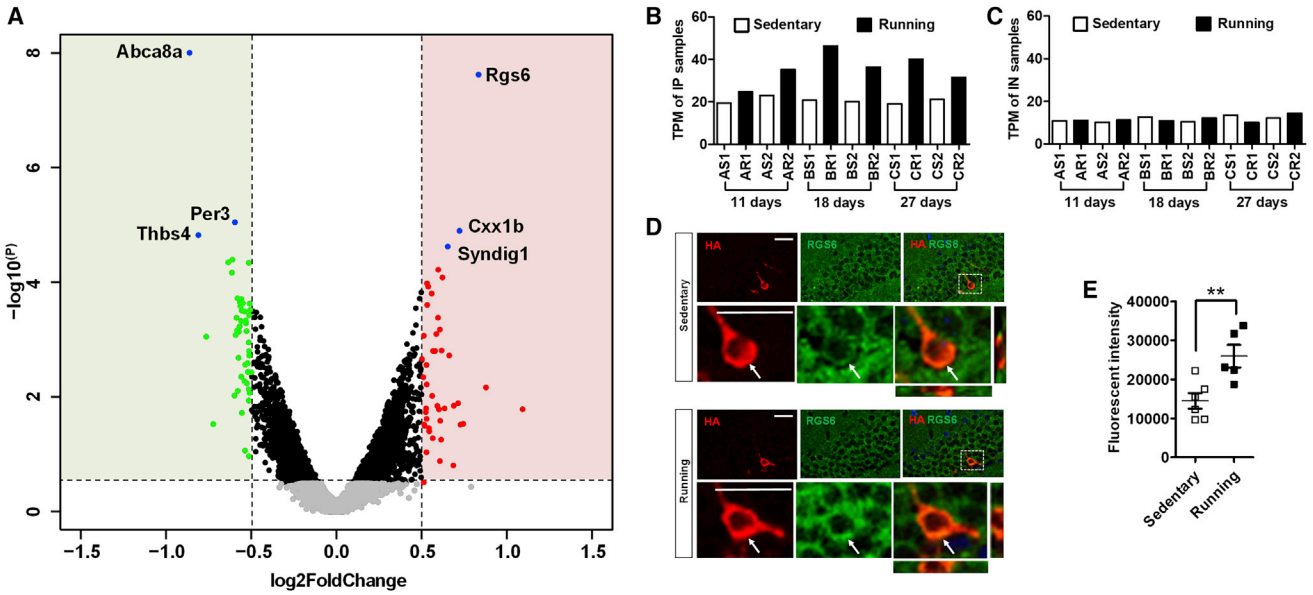

Figure 3. Adult Newborn Neurons in Running Mice Have Increased RGS6 Levels

(A) A volcano plot showing DEGs between running and sedentary groups. Genes with more than 1.5-fold change (>1.5-fold or <−1.5-fold) and p value (<0.05) were indicated with color (green, downregulated; red, upregulated in running).

(B and C) RNA-seq TPM (transcripts per million) values showed *Rgs6* levels were increased in the IP (B), but not in the IN, samples (C) in running mice compared with sedentary mice.

(D) Sample confocal images used for quantitative analysis in (F) showing RGS6 (green) and HA (red) immunoreactivities in the DG of sedentary and running Nes-HA mice. Scale bar, 25 μm.

(E) Quantitative results of RGS6 protein levels in the HA^+ cells in 18-day sedentary (n = 6) and running (n = 5) mice (**p < 0.01, t test).

and substance abuse (Figure 2E). Therefore, the new neurons mount dynamic and development-stage-specific gene expression changes in response to voluntary running, and many of these genes are important for neuronal development and functions.

Next, we asked whether gene expression changes were dynamic across time points. We performed gene co-expression network analysis using WGCNA and clustered genes into co-expression modules (Langfelder and Horvath, 2008). The genes with similar temporal expression dynamics were clustered together in the same module (e.g., select modules in Figure 2F; Figure S2I). In total, we identified 92 modules (Figure S2I) and 23 modules that exhibited most different expression dynamics between running and sedentary controls, as shown by modular eigengenes (Figure 2F). For example, some modules (e.g., M53, M59, M85) showed dramatic upregulation in the sedentary mice but downregulation in running mice from 11 to 27 days. In contrast, some modules (e.g., M1, M23, M36) showed dramatic upregulation in the running mice, but not in the sedentary mice, from 11 to 27 days (Figure 2F). These results demonstrate dynamic changes of gene expression during maturation that are differentially affected in running and sedentary mice.

To further identify the biological functions related to running-specific expression dynamics, we also identified enriched pathways in gene co-expression modules (Table S3). Several running-specific modules have enriched neurogenesis-related biological processes, for example, module M5 genes were enriched with neuron differentiation, neurogenesis, and neuron projection guidance, and M92 genes were enriched with neurogenesis (Figure 2G). A number of biological processes, including cellular protein localization, symbiotic process, and cellular localization, were associated with enriched genes in M76. In addition, genes in modules M13 and M42 were associated with biological processes nitrogen compound metabolic process and cellular metabolic process, respectively. These results revealed dynamic regulations of biological processes during maturation of the adult-born new neurons and differential dynamic changes in running and sedentary mice. In summary, adult-born DG new neurons exhibit intrinsic dramatic changes in response to running, and these changes correspond to an accelerated maturation.

Running Elevates RGS6 Expression in Adult Newborn Neurons

Several genes exhibited significant changes in adult newborn neurons across all three time points (Figure 3A). The top down-regulated gene was *Abca8a*, a mouse ortholog gene of human *ABCA8* (ATP Binding Cassette Subfamily A Member 8). *Abca8a* was downregulated in both IP and IN. The top upregulated gene was *Rgs6*, which was specifically upregulated in IP, but not in the IN, of running mice (Figures 3B and 3C), suggesting that RGS6 might mediate the adult-born new neurons-specific response to running. We therefore decided to further assess the roles of RGS6 upregulation in running-induced neurogenesis. We first assessed the expression patterns of RGS6 during adult neurogenesis. We found that RGS6 protein was low in radial glia-like ($GFAP^+NESTIN^+$) NSCs and ($NESTIN^+$ or $Ki67^+$) IPCs, but was

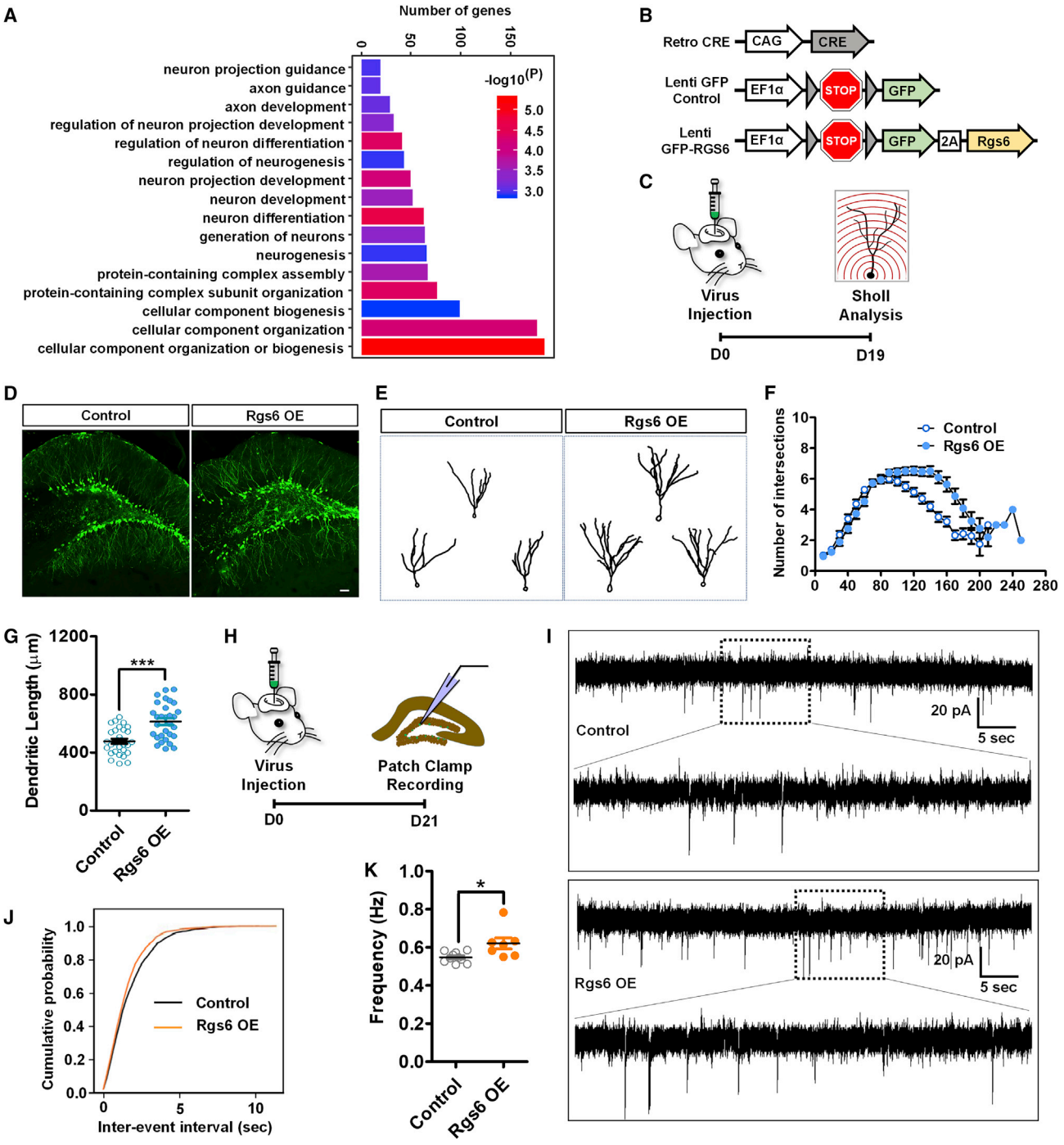

Figure 4. Enhancing RGS6 Levels in Adult-Born Neurons Promotes Neuronal Maturation

(A) GO analysis of *Rgs6* (M5) module genes.

(B) A schematic illustration of viral vectors used for *in vivo* targeting of adult new neurons: retroviral vector expressing Cre recombinase (Retro-CRE), lentiviral vector with CRE-dependent expression of GFP (Lenti-GFP-Control), and lentiviral vector with CRE-dependent expression of GFP-RGS6 (Lenti-GFP-RGS6).

(C) Timeline of *in vivo* viral targeting for morphological analysis of adult-born new neurons.

(D) Sample confocal images of virus-infected adult new neurons. Scale bar, 50 μm.

(E) Sample traces of GFP-expressing neurons.

(F) Overexpression of RGS6 increases the dendritic complexity compared with controls [$F(1,60) = 26.357$, $p < 0.001$, multivariate analysis of variance (MANOVA)].

(G) Exogenous expression of RGS6 increases dendritic length of adult new neurons compared with controls ($p < 0.0001$, t test).

(H) Timeline of *in vivo* viral targeting for electrophysiological analysis of adult-born new neurons.

(legend continued on next page)

expressed in both DCX^+ immature neurons and $NeuN^+$ mature neurons (Figures S3A–S3D), suggesting a functional role of RGS6 in neurons (Figures S3C and S3D). Indeed, RGS6 protein levels were upregulated in HA^+ new neurons in 18-day running mice compared with controls (Figures 3D and 3E). RGS6 belongs to the R7-Rgs subfamily of RGS proteins that accelerate the GTPase activity of $G_{(i/o)}$ class of Gα to terminate signaling cascades of G protein-coupled receptors (GPCRs) (Ross and Wilkie, 2000). RGS6 is enriched in both hippocampal and cortical neurons (Stewart et al., 2014) and has been shown to modulate $GABA_B$ receptor signaling (Maity et al., 2012) that inhibits adult neurogenesis (Giachino et al., 2014). However, whether RGS6 plays a role in any of the biological processes in adult-born new neurons has never been investigated.

Enhancing RGS6 Expression in Adult-Born New Neurons Promotes Neuronal Maturation

To determine the potential neurogenic functions of elevated RGS6 in adult-born neurons, we performed GO analysis of all the genes within the eigengenes-module M5 that contains *Rgs6* (Table S3). Interestingly, the most significant biological processes generated from M5 module genes were related to neuronal maturation (Figure 4A). Because running enhances morphological maturation in running mice (Steib et al., 2014), we hypothesized that increased levels of RGS6 in new neurons played a role in running-enhanced neuronal maturation.

Multiple RGS6 protein isoforms resulted from alternative splicing. Although the antibody we used (Figure 3D) recognized all major RGS6 isoforms, only one *Rgs6* isoform, equivalent to the human alpha2 long RGS6 isoform (RGS6Lα2; GenBank: AH011570.2) (Chatterjee et al., 2003) was highly expressed in adult-born neurons and was also differentially expressed between running and sedentary conditions (Figure S4A). We next overexpressed RGS6Lα2 in adult new neurons using lentivirus vectors expressing either RGS6 (GFP-RGS6) or GFP alone (control) in a Cre-dependent manner, together with retrovirus-expressing Cre into the adult DG (Figures 4B and 4C; Figures S4B and S4C). Only dividing adult NSCs or IPCs could be targeted by retrovirus. RGS6 OE did not significantly impact NPC proliferation (Figure S5; Figures 4D and 4E). We found that at 19 days after viral injection, newborn neurons expressing GFP-RGS6 showed increased dendritic complexity and total dendritic length compared with neurons expressing GFP alone (Figures 4D–4G). Therefore, increased RGS6 levels in adult-born new neurons of sedentary mice leads to enhanced dendritic maturation.

Adult new neurons exhibit electrophysiological changes reflecting maturation stages (Ge et al., 2006; Trinchero et al., 2019). We performed whole-cell patch-clamp recording at 3 weeks post-viral injection (Figure 4H). New neurons infected with GFP-RGS6 virus exhibited increased frequency of miniature excitatory postsynaptic currents (mEPSCs) compared with new neurons infected with GFP virus (Figures 4I–4K). Taken together, increased expression levels of RGS6 in adult-born neurons in sedentary mice mimics the effect of running on neuronal maturation in running mice.

Enhancing RGS6 Expression in Adult-Born Neurons Reduces Their Sensitivity to $GABA_B$ Receptor Activation

RGS6 accelerates the GTPase activity of $G_{(i/o)}$ to terminate GPCR signaling (Ross and Wilkie, 2000). In fact, "regulation of GTPase activity" and "GTPase binding" GO terms were identified in 508 unique DEGs of 27-day IP samples, but not IN samples (Table S2). Prior studies have shown that RGS6 modulates signaling by the $GABA_B$ receptor (Maity et al., 2012). We found that GABA-related GO terms were identified in 508 unique DEGs 27-day IP samples, but not in IN samples (Table S2). $GABA_B$ receptor activation is known to inhibit maturation of adult hippocampal new neurons (Giachino et al., 2014). We hypothesized that running-induced upregulation of RGS6 in adult-born immature neurons renders them less sensitive to $GABA_B$ receptor activation (Figure 5A). Downstream effects of $GABA_B$ receptor activation include activation of G protein-gated inwardly rectifying K^+ channels (GIRKs) and inhibition of voltage-gated Ca^{2+} channels (VGCCs) (Hollinger and Hepler, 2002; Padgett and Slesinger, 2010). Because immature adult-born neurons initially lacked functional GIRK signaling (Gonzalez et al., 2018), we assessed the strength of $GABA_B$-receptor-mediated suppression of VGCCs by the $GABA_B$ receptor agonist baclofen. We first tested whether voluntary running altered baclofen-induced suppression of VGCCs, using Ascl1-CreERT2::Rosa26-STOP-TdTomato (Ascl1-tdT) mice to identify adult-born neurons (Yang et al., 2015; Figure S6). After Tam induction, Ascl1-tdT mice were exposed to running wheels or locked wheels for 22–26 days, and then we recorded pharmacologically isolated Ca^{2+} currents in tdT^+ adult-born neurons (Figure 5B). In sedentary mice, baclofen (30 μM) reduced the peak Ca^{2+} current to 41% ± 8% of control (Figure 5C). On the contrary, in running mice, baclofen did not significantly reduce peak Ca^{2+} currents (81% ± 10% of control; Figure 5D). This result suggests that running renders adult new neurons less sensitive to $GABA_B$-receptor-mediated suppression of neuronal activation.

Next, we assessed whether elevated RGS6 contributed to the running-induced reduction in $GABA_B$-receptor-mediated signaling using the same viral targeting strategy (Figure 5E). In mice expressing control GFP, baclofen (30 μM) uniformly reduced peak Ca^{2+} currents to 73% ± 5% of control (Figure 5F), whereas in mice targeted with RGS6 OE, baclofen did not significantly reduce peak Ca^{2+} currents (101% ± 3% of control; Figure 5G). Hence elevating expression of RGS6 specifically in adult-born immature neurons rendered them less sensitive to $GABA_B$ receptor activation. Therefore, both running mice with elevated RGS6 in adult neurons and targeted RGS6 OE in adult new neurons indicate that RGS6 OE suppresses $GABA_B$-receptor-mediated G protein signaling.

(I) Representative traces of mEPSCs recorded from GFP^+ new neurons in acute hippocampal slices derived from control and RGS6 OE mice 3 weeks after retroviral injection.

(J and K) Cumulative probability distribution (J) and frequency (K) (control, n = 10 cells; RGS6 OE, n = 7 cells) and average frequency ($p = 0.0154$, two-tailed t test). *$p < 0.05$, **$p < 0.01$, ***$p < 0.001$.

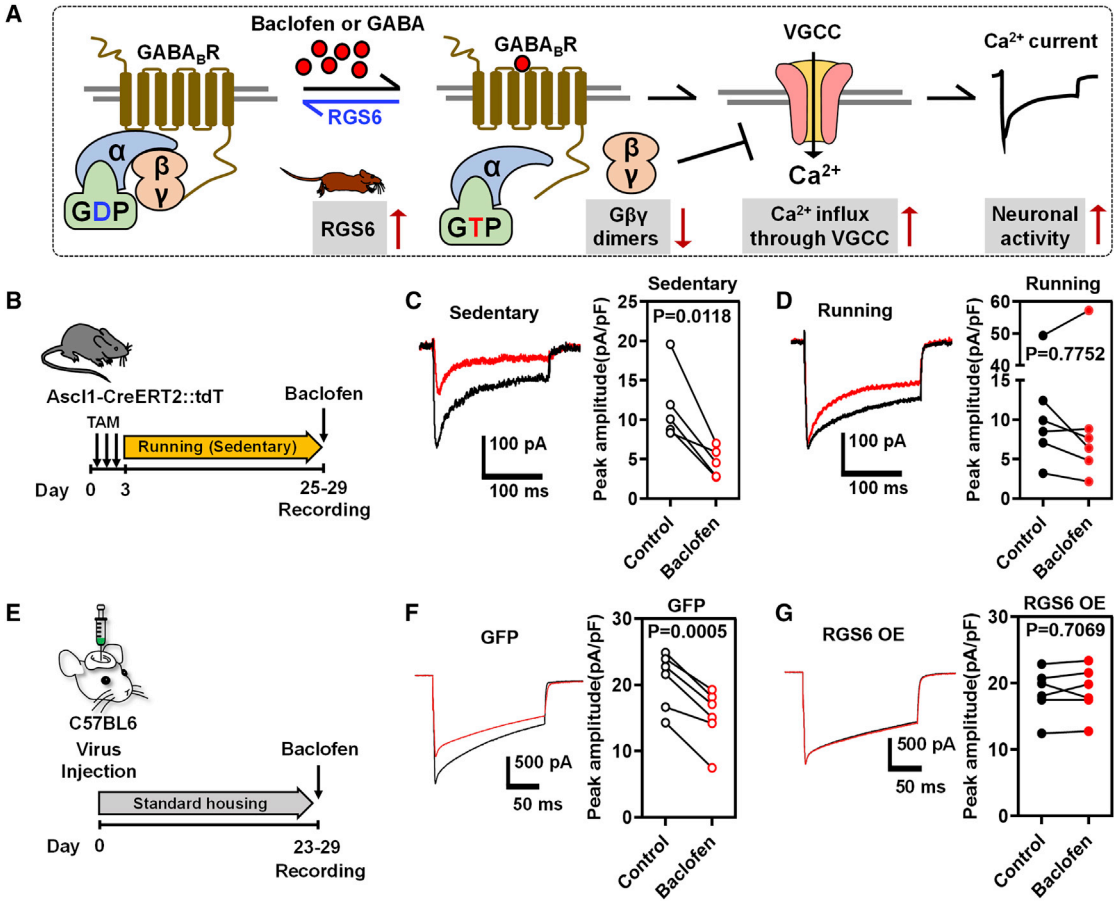

Figure 5. Both Voluntary Running and Elevating RGS6 Expression Levels in Adult-Born Neurons Reduce Their Sensitivity to $GABA_B$-Receptor-Mediated Inhibition

(A) Hypothetic model for the role of RGS6 in reduced sensitivity to $GABA_B$ receptor signaling in running mice. $GABA_B$ receptor activation by GABA or baclofen leads to activation of Gα and dissociation of Gβγ subunits from the trimeric G protein complex. Gβγ is inhibitory to voltage-gated calcium channel (VGCC) in adult new neurons. Elevated RGS6 accelerates GTP hydrolysis and therefore terminates $GABA_B$ receptor activation and relieves the inhibitory effects on VGCC, rendering adult new neurons less sensitive to GABA or baclofen-activated $GABA_B$ signaling.

(B) Experimental timeline for testing the efficiency of the $GABA_B$ agonist baclofen on suppression of Ca^{2+} currents in immature GCs (granule cells) in sedentary and running mice.

(C and D) Average traces (left) of baclofen-induced (30 μM, red) suppression of peak Ca^{2+} currents recorded in immature neurons from sedentary (C) and running (D) mice. In sedentary mice (C, right), baclofen reduced the peak current from 11.7 ± 2.3 to 4.6 ± 0.9 pA/pF (n = 5; p = 0.01, paired t test), whereas baclofen had no significant effect on currents in running mice (15.1 ± 7 to 14.5 ± 8.6 pA/pF; n = 6; p = 0.8, paired t test) (D, right).

(E) Experimental timeline for testing the efficiency of baclofen on suppression of Ca^{2+} currents in immature GCs in GFP (GFP only control) and RGS6 OE (RGS6 overexpression) mice.

(F and G) Left: examples of baclofen-induced (30 μM, red) suppression of peak Ca^{2+} currents recorded from control GFP immature GCs (F) or RGS6 OE immature GCs (G). Right: in control GFP immature GCs, baclofen reduced the peak Ca^{2+} current from 20.7 ± 1.7 to 15.2 ± 1.7 pA/pF (n = 6; p < 0.001, paired t test). In RGS6 OE immature GCs, baclofen did not affect Ca^{2+} currents (18.6 ± 1.4 to 18.8 ± 1.5 pA/pF; n = 6; p = 0.7).

RGS6 Is Required for Running-Enhanced Maturation of Adult-Born New Neurons

We next assessed whether RGS6 is necessary for running-enhanced neuronal maturation. We targeted adult-born neurons using retrovirus expressing either control short hairpin RNA (shRNA) (*shNC*) or *shRgs6* (Figure S7), as well as GFP. We first subjected *shNC* retrovirus-injected mice to either voluntary running or sedentary conditions for 17 days (Figures 6A and 6B). GFP^+ newborn neurons in running mice showed significant increase in dendritic complexity and total dendritic length (Figures 6C–6F), consistent with the literature (Steib et al., 2014). We then subjected *shRgs6*-injected mice to either running or sedentary treatment for 17 days. Newborn neurons with RGS6 knockdown did not show significant differences in either dendritic complexity or dendritic length (Figures 6G–6I) between running and sedentary conditions. Therefore, RGS6 is a necessary mediator for running-induced neuronal dendritic maturation.

To further assess the role that RGS6 upregulation played in neuronal maturation, we performed whole-cell patch-clamp recording of immature neurons infected with retroviral *shRgs6* or *shNC* (shRNA control) in the running mice (Figure 6J). The frequency of mEPSCs recorded from RGS6 knockdown cells was

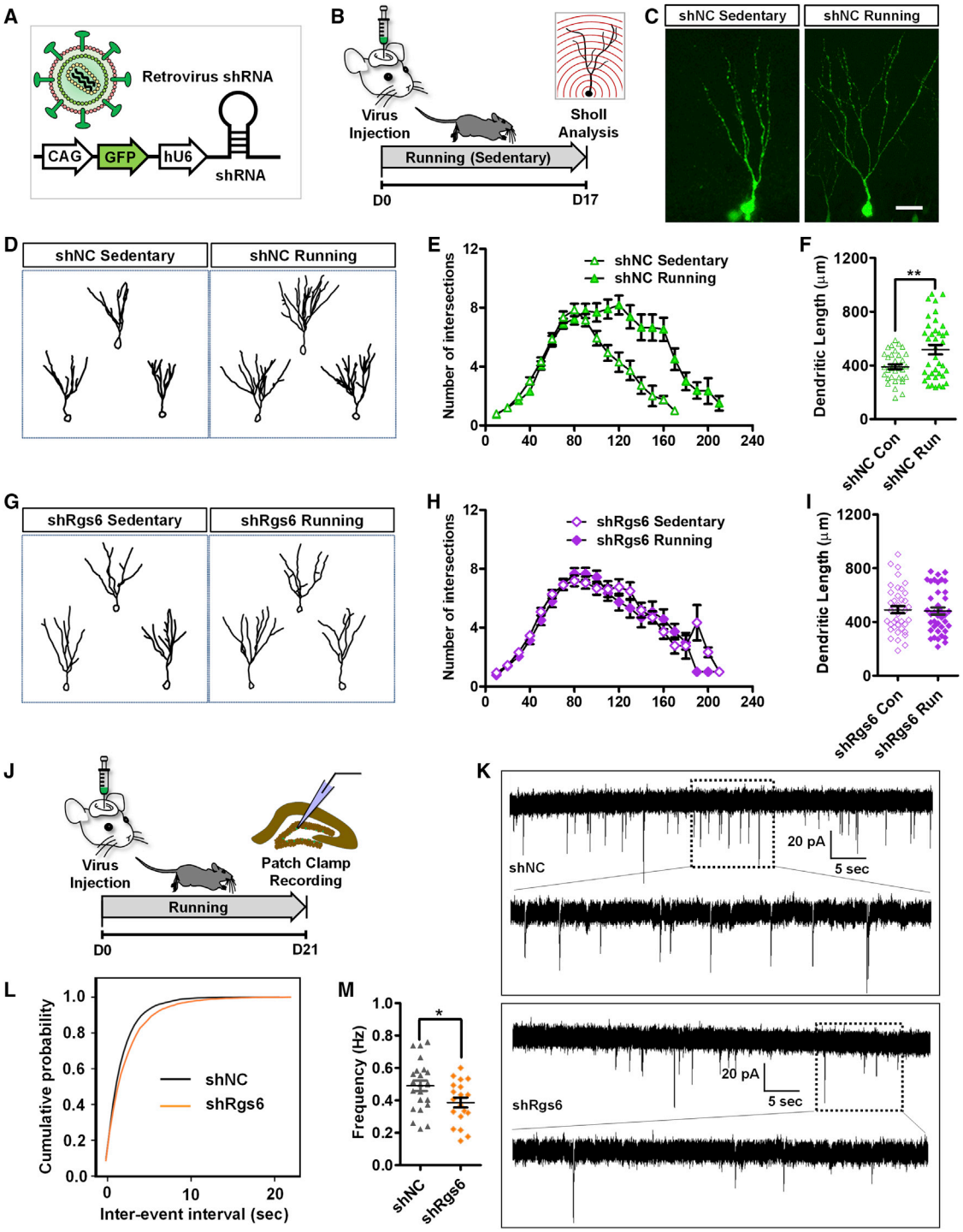

Figure 6. Knockdown of RGS6 in Adult-Born New Neurons Abolishes the Running Effect on New Neuron Maturation

(A) A schematic illustration of retroviral vector expressing shRNA and GFP for targeting adult new neurons.

(B) Experimental timeline for accessing the effect of RGS6 knockdown on dendritic morphology of adult new neurons in running and sedentary mice.

(C) Sample confocal images of virus-infected and GFP$^+$ neurons. Scale bar, 50 μm.

(D) Sample traces of retrovirus shNC-infected neurons in running and sedentary mice.

(E) Running increases dendritic complexity of adult-born new neurons in mice injected with control shNC virus [$F(1,72) = 9.241$; $p < 0.01$, MANOVA].

(F) Running increases the dendritic length of adult-born new neurons ($p < 0.01$, t test).

(legend continued on next page)

significantly decreased compared with those in controls (Figures 6K–6M). These results suggest that RGS6 knockdown in immature neurons abolishes the running effects of elevated ability to receive excitatory transmission, which may result from dendritic maturation deficits. Therefore, RGS6 is essential for running effects on neuronal maturation.

RGS6 Is Required for Running-Enhanced Hippocampal-Dependent Learning Ability and Anxiolytic Effect

Voluntary running enhances both spatial and associative learning (reviewed by Eisinger and Zhao, 2018; Vivar et al., 2013), as well as exerts an anxiolytic effect (Schoenfeld et al., 2016) in rodents. We first injected control lentivirus into the DG of adult mice, housed them with either running or locked wheels for 4 weeks, and subjected them to several tests that have been used to demonstrate running-induced behavioral changes, including novel location test for spatial learning (Snigdha et al., 2014), contextual fear conditioning for associative learning (Lin et al., 2012), and elevated plus maze for anxiety (Schoenfeld et al., 2016). We found that running mice exhibited reduced anxiety (Figures 7B and 7C) and enhanced spatial and contextual learning, compared with sedentary mice (Figures 7E, 7F, 7H, and 7I), which was consistent with the literature (Lin et al., 2012; Schoenfeld et al., 2016; Snigdha et al., 2014). We then injected another cohort of adult mice with virus expressing either *shNC* or *shRgs6* and then subjected both groups of mice to running followed by the same behavioral tests. We found that *shRgs6* virus-injected mice had higher levels of anxiety and reduced spatial and contextual learning performance compared with *shNC* virus-infected mice (Figures 7D, 7G, and 7J). In fact, running mice injected with *shRgs6* virus exhibited similar levels of learning ability as the sedentary mice injected with control *shNC* virus (Figures 7C, 7D, 7F, 7G, 7I, and 7J). Therefore, RGS6 is required for running-induced adult-born new neuron maturation and hippocampal neurogenesis-dependent learning enhancement and anxiolytic effect.

DISCUSSION

We have discovered that, in response to voluntary running, adult-born new neurons in the DG mount dynamic translational changes that are distinct from those of other cell types within the DG tissue, with genes important for neuronal maturation dramatically differentially expressed in new neurons, but not in DG tissue. We demonstrated that *Rgs6* has an important role in running-induced new neuron maturation and behavioral improvements. Therefore, our study has provided a genome-wide view of intrinsic molecular changes in the adult newborn neurons and unveils a molecular mechanism underlying voluntary running-induced neurogenesis.

Adult hippocampal neurogenesis is sensitive to external stimuli and experiences, a feature that is important for both understanding diseases and developing therapeutics. Some of the most effective positive stimuli for adult neurogenesis include voluntary running and enriched environment (Kempermann, 2015). Since the first publications on positive effects of running on adult neurogenesis (Kempermann et al., 1997; van Praag et al., 1999), significant interest and effort have been dedicated to understanding the underlying molecular mechanisms. To date, at least 10 research groups have used either microarray or RNA sequencing to interrogate the hippocampal or DG tissues in rodent models subjected to running wheels and post-mortem hippocampal tissues from humans who have been physically active for at least two decades (Berchtold et al., 2019; Chatzi et al., 2019; Eisinger and Zhao, 2018; Grégoire et al., 2018). However, none of these studies has assessed genome-wide changes specifically in adult-born new neurons in response to voluntary running. Our study has therefore filled this gap of knowledge.

Adult-born immature neurons represent an extremely small portion of the total cell population in the DG, therefore, assessing intrinsic changes in adult neurons is difficult using dissected hippocampal and DG tissues. A number of new methods have been applied to isolate new neurons from the adult DG, including cell sorting used by several others and us (Gao et al., 2017; Shin et al., 2015; Bracko et al., 2012). However, tissue dissociation may cause extensive cellular stress, especially to neurons (Habib et al., 2016). The adult new neuron-specific RiboTag-seq used here does not require dissociation of live cells and therefore avoids confound of disruptive cell isolation. This method proves powerful in identifying intrinsic genome-wide molecular changes in adult new neurons, as well as other small numbers of cells in mature tissues. As a future direction, it would be informative to assess the impact of an enriched environment, aging, and disease mutations on translational responses of adult new neurons using this method and compare with the effect of running. A limitation of our method is that the HA-labeled cells contain adult-born new cells that are not exactly at the same developmental stages. Single-cell analysis of directly isolated adult Nestin$^+$ NPCs (Shin et al., 2015) and DCX$^+$ immature neurons (Gao et al., 2017) has been used to assess developmental progression of these new cells, but tissue dissociation may not recover mRNA localized in dendrites. In addition, the read coverage of single-cell analysis remains limited, prohibiting the identification of some low-expressing regulators. RiboTag-seq at single-cell levels has not yet been developed.

RGS6 belongs to a group of RGS proteins that regulate G protein activity, which, in turn, modulates the activity of neurotransmitter receptors and diverse signaling pathways, including those associated with cell growth and differentiation

(G–I) RGS6 knockdown abolishes running-induced increased dendritic complexity [shRgs6-sedentary versus shRgs6-running; $F(1,80) = 0.23$; $p = 0.633$, M-ANOVA] and increased dendritic length ($p > 0.05$, t test). (G) Sample traces of viral targeted neurons. Sholl analysis shows no significant difference in both number of intersections (H) and dendritic length (I) between groups.

(J) Experimental timeline for patch-clamp recording of adult-born new neurons with RGS6 knockdown.

(K) Representative traces of mEPSCs recorded from GFP$^+$ DG neurons in acute hippocampal slices derived from *shNC* and shRgs6 mice 3 weeks after retroviral injection.

(L and M) Cumulative probability distribution (L) and frequency (M) (*shNC*, n = 23 cells; *shRgs6*, n = 19 cells) and average frequency ($p = 0.0259$, t test). *$p < 0.05$, **$p < 0.01$, ***$p < 0.001$.

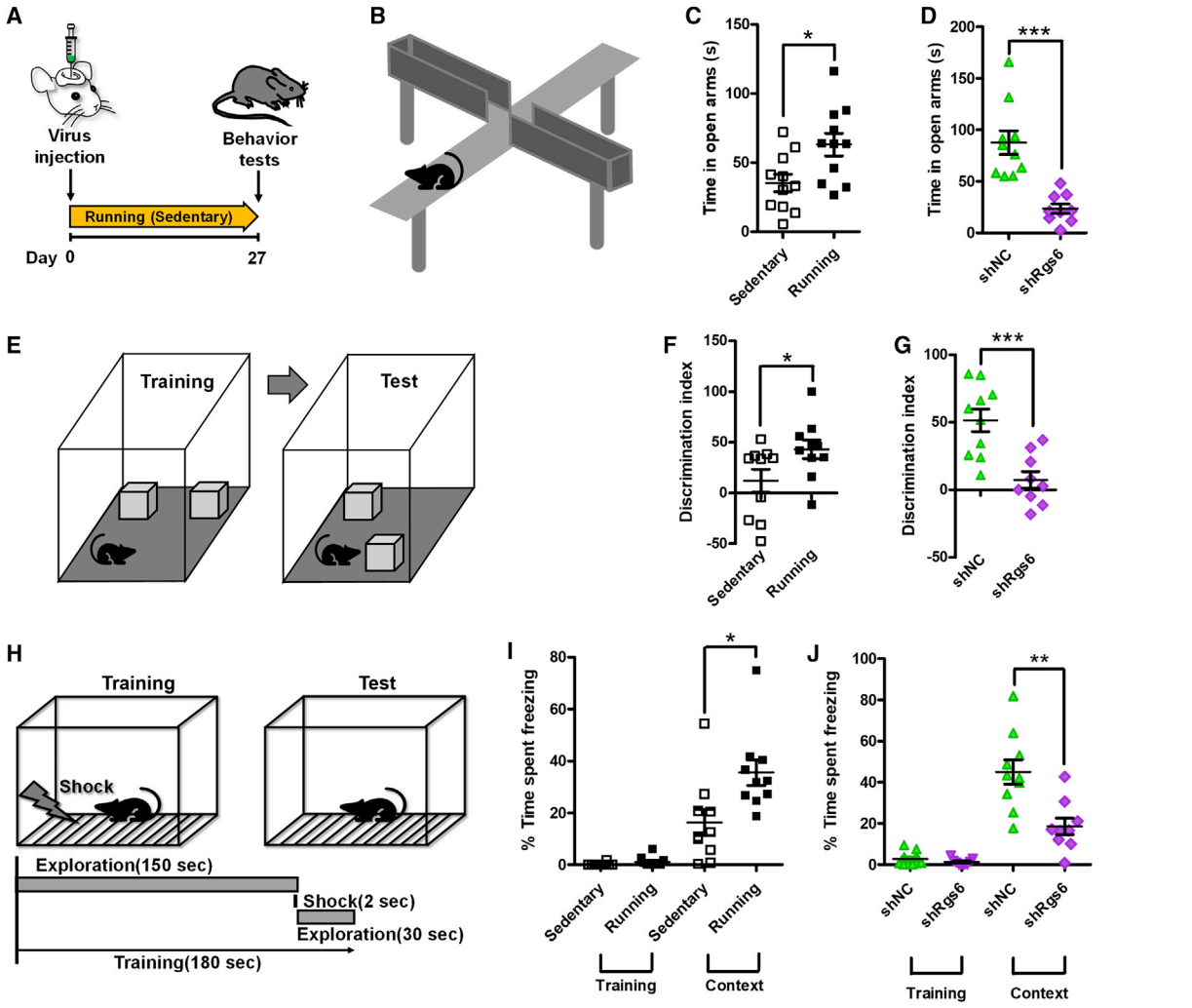

Figure 7. RGS6 Is Required for Running-Induced Learning and Memory Enhancement and Anxiolytic Effect

(A) Experimental timeline for assessing the effect of RGS6 knockdown on anxiety, spatial learning, and memory in running and sedentary mice.

(B) A scheme cartoon illustrates elevated plus maze (EPM) test.

(C) Running mice exhibit reduced anxiety compared with sedentary mice as measured using an EPM test ($p = 0.0141$; sedentary: 35.22 ± 6.25; running: 63.02 ± 8.21).

(D) Knockdown of Rgs6 abolishes running-induced reduced anxiety in running mice ($p = 0.0001$, *shNC*: 87.60 ± 11.46; *shRgs6*: 23.51 ± 4.73).

(E) A scheme cartoon illustrates novel location test (NLT).

(F) Running mice exhibit improved spatial learning compared with sedentary mice measured by NLT ($p = 0.0485$; sedentary: 12.07 ± 11.38; running: 43.08 ± 9.233).

(G) Knockdown of RGS6 abolishes running-induced improvement on spatial learning in running mice ($p = 0.0007$; *shNC*: 51.46 ± 8.36; *shRgs6*: 7.27 ± 6.27).

(H) A scheme cartoon illustrates contextual fear conditioning test.

(I) Running mice exhibit improved contextual learning compared with sedentary mice measured by a contextual fear conditioning test ($p = 0.014$; sedentary: 16.35 ± 5.05; running: 35.54 ± 4.93).

(J) RGS6 knockdown abolishes running-induced improvement on contextual learning in running mice ($p = 0.0021$; *shNC*: 45.01 ± 5.85; *shRgs6*: 18.61 ± 4.04). *$p < 0.05$, **$p < 0.01$, ***$p < 0.001$. Data are presented as mean ± SEM.

(Hollinger and Hepler, 2002). Among RGS proteins, RGS6, RGS7, and RGS11 share homology and targets (Anderson et al., 2009). However, only RGS6 was upregulated in running mice. In addition, although both adult new neurons and mature neurons express RGS6, RGS6 upregulation was specific to adult-born new neuron. Furthermore, upregulation of RGS6 and knockdown of RGS6 in adult new neurons had significant impact on morphology and excitability of new neurons, which have been shown to significantly impact behaviors (Gonçalves et al., 2016). Therefore, the behavioral deficits we observed in running mice with RGS6 knockdown likely, if not solely, resulted from RGS6 reduction in adult new neurons rather than other cell types in the DG. Our results also point to a possible explanation for the role of RGS6 in activity-dependent new neuron maturation. GABAergic mechanisms contribute to activity-dependent modulation of adult neurogenesis via both

$GABA_A$ and $GABA_B$ receptors. RGS6 inhibits the $GABA_B$-GIRK signaling pathway by accelerating deactivation of Gα and reducing the availability of free Gβγ (Hollinger and Hepler, 2002; Maity et al., 2012; Padgett and Slesinger, 2010). Although $GABA_B$-GIRK signaling is a well-known target of RGS6, the late development of functional GIRK channels during adult neurogenesis makes it unlikely to mediate RGS6 effects on running-induced maturation (Gonzalez et al., 2018). Regulation of VGCCs is more likely to mediate activity-dependent regulation at early stages of maturation, when depolarization generates Ca^{2+} influx that is important for many intracellular signaling pathways regulating neurodevelopment, including dendrite arborization (Chevaleyre et al., 2002; Greer and Greenberg, 2008; Rajan and Cline, 1998; Wong and Ghosh, 2002). In adult-born neurons, Ca^{2+} influx generated by $GABA_A$ receptor depolarization is thought to promote activity-dependent development (Ge et al., 2007). Our data suggest that RGS6 could promote neuronal maturation by releasing the inhibitory effect of $GABA_B$ receptor signaling on voltage-activated Ca^{2+} influx (Figure 5), potentially providing a synergistic interaction with $GABA_A$-mediated depolarization. It would be interesting for future studies to investigate this interaction, as well as to investigate how running leads to elevated RGS6 in adult new neurons. In addition, our current investigation has focused on how upregulation of RGS6 in new neurons of running mice promoted neuronal maturation. It would be interesting to further investigate how RGS6 and specific isoforms of RGS6 regulate functions of neurons both with and without external stimuli.

Because our IN data are essentially transcriptome of the DG tissues, we compared our 27-day IN data with the only DG RNA-seq dataset from the 28-day running CD1 strain of mice (Grégoire et al., 2018). We found that 25 of 124 of our downregulated and 18 of 124 of our upregulated DEGs overlapped with published DEGs; however, most (~80%) of our DEGs were not shared with the published DEGs. This difference could be because of different genetic background and tissue-processing methods. In addition, we found that different sets of genes in IN samples responded to voluntary running. The genes upregulated in IN of 11-day running mice are associated with synaptic related biological process GO terms, such as chemical synaptic transmission (Table S4). Because at 11 days most new neurons are quite immature, these synaptic changes in the IN likely represent the early response of mature neurons. Interestingly, genes upregulated in IN of longer-period running (18 and 27 days) do not seem to contribute to synaptic changes. Therefore, our data demonstrate that mature DG neurons and adult-born new neurons mount different gene expression responses in response to voluntary running.

In conclusion, our study has provided a genome-wide view of intrinsic molecular changes in the adult newborn neurons that contribute to voluntary running-induced neurogenesis. The mediators we have identified, such as RGS6, may have the potential to serve as therapeutic targets for neurodegenerative diseases and aging.

STAR★METHODS

Detailed methods are provided in the online version of this paper and include the following:

SUPPLEMENTAL INFORMATION

Supplemental Information can be found online at https://doi.org/10.1016/j.celrep.2020.107997.

ACKNOWLEDGMENTS

We thank Y. Xing, R. Spitzer, D. Wagner, A. Meara, S. Pham, Y. Choi, K. Schoeller, J. Le, M. Syed, M. Seelig, and Y. Sun for technical assistance; J. Pinnow, M. Eastwood, D. Bollig, and K. Knobel at the Waisman Intellectual and Developmental Disabilities (IDD) Model Core; and S. Splinter-BonDurant at the University of Wisconsin(UW)-Madison Biotechnology Center for next generation sequencing services. This work was supported by grants from the National Institutes of Health (R01NS105200, R56MH113146, R01MH116582, and R21NS095632 to X.Z.; R01HD064743 to Q.C.; R01NS064025 and R01NS105438 to L.O.-W.; R01AG067025 and U01MH116492 to D.W.; U54HD090256 to the Waisman Center), American Epilepsy Society postdoctoral fellowship (to J.C.G.), UW Vilas Trust (Mid-Career Award), Wisconsin Alumni Research Foundation, and Jenni and Kyle Professorship (to X.Z.).

AUTHOR CONTRIBUTIONS

X.Z. conceived the concept and designed experiments. Y.G. designed and performed experiments, collected data, and analyzed data. Y.G. and X.Z. wrote the manuscript. Y.G. and B.E.E. performed bioinformatics analysis. D.W (daifeng.wang@wisc.edu) performed pseudotime and coexpression network analysis. S.K., J.T.H., J.P., and S.J. collected data. J.C.G. and L.O.-W. designed and performed electrophysiological analyses for Ca^{2+} current recording. M.S. performed behavioral tests. Q.D. and Q.C. designed and performed electrophysiological analyses for mEPSCs.

DECLARATION OF INTERESTS

The authors declare no competing interests.

Received: April 21, 2020
Revised: June 29, 2020
Accepted: July 15, 2020
Published: August 4, 2020; Corrected online: August 12, 2020

REFERENCES

Aimone, J.B., Deng, W., and Gage, F.H. (2010). Adult neurogenesis: integrating theories and separating functions. Trends Cogn. Sci. *14*, 325–337.

Allan, A.M., Liang, X., Luo, Y., Pak, C., Li, X., Szulwach, K.E., Chen, D., Jin, P., and Zhao, X. (2008). The loss of methyl-CpG binding protein 1 leads to autism-like behavioral deficits. Hum. Mol. Genet. *17*, 2047–2057.

Anderson, G.R., Posokhova, E., and Martemyanov, K.A. (2009). The R7 RGS protein family: multi-subunit regulators of neuronal G protein signaling. Cell Biochem. Biophys. *54*, 33–46.

Basu, S.N., Kollu, R., and Banerjee-Basu, S. (2009). AutDB: a gene reference resource for autism research. Nucleic acids research *37*, D832–D836.

Berchtold, N.C., Prieto, G.A., Phelan, M., Gillen, D.L., Baldi, P., Bennett, D.A., Buchman, A.S., and Cotman, C.W. (2019). Hippocampal gene expression patterns linked to late-life physical activity oppose age and AD-related transcriptional decline. Neurobiol. Aging *78*, 142–154.

Bracko, O., Singer, T., Aigner, S., Knobloch, M., Winner, B., Ray, J., Clemenson, G.D., Jr., Suh, H., Couillard-Despres, S., Aigner, L., et al. (2012). Gene expression profiling of neural stem cells and their neuronal progeny reveals IGF2 as a regulator of adult hippocampal neurogenesis. The Journal of neuroscience : the official journal of the Society for Neuroscience *32*, 3376–3387.

Brandt, M.D., Jessberger, S., Steiner, B., Kronenberg, G., Reuter, K., Bick-Sander, A., von der Behrens, W., and Kempermann, G. (2003). Transient calretinin expression defines early postmitotic step of neuronal differentiation in adult hippocampal neurogenesis of mice. Molecular and cellular neurosciences *24*, 603–613.

Chatterjee, T.K., Liu, Z., and Fisher, R.A. (2003). Human RGS6 gene structure, complex alternative splicing, and role of N terminus and G protein gamma-subunit-like (GGL) domain in subcellular localization of RGS6 splice variants. J. Biol. Chem. *278*, 30261–30271.

Chatzi, C., Zhang, Y., Hendricks, W.D., Chen, Y., Schnell, E., Goodman, R.H., and Westbrook, G.L. (2019). Exercise-induced enhancement of synaptic function triggered by the inverse BAR protein, Mtss1L. eLife *8*, e45920.

Chevaleyre, V., Moos, F.C., and Desarménien, M.G. (2002). Interplay between presynaptic and postsynaptic activities is required for dendritic plasticity and synaptogenesis in the supraoptic nucleus. J. Neurosci. *22*, 265–273.

Christian, K.M., Song, H., and Ming, G.L. (2014). Functions and dysfunctions of adult hippocampal neurogenesis. Annu. Rev. Neurosci. *37*, 243–262.

Deng, W., Aimone, J.B., and Gage, F.H. (2010). New neurons and new memories: how does adult hippocampal neurogenesis affect learning and memory? Nat. Rev. Neurosci. *11*, 339–350.

Deshpande, A., Bergami, M., Ghanem, A., Conzelmann, K.K., Lepier, A., Götz, M., and Berninger, B. (2013). Retrograde monosynaptic tracing reveals the temporal evolution of inputs onto new neurons in the adult dentate gyrus and olfactory bulb. Proc. Natl. Acad. Sci. USA *110*, E1152–E1161.

Dong, J., Pan, Y.B., Wu, X.R., He, L.N., Liu, X.D., Feng, D.F., Xu, T.L., Sun, S., and Xu, N.J. (2019). A neuronal molecular switch through cell-cell contact that regulates quiescent neural stem cells. Sci. Adv. *5*, eaav4416.

Eadie, B.D., Redila, V.A., and Christie, B.R. (2005). Voluntary exercise alters the cytoarchitecture of the adult dentate gyrus by increasing cellular proliferation, dendritic complexity, and spine density. J. Comp. Neurol. *486*, 39–47.

Eisinger, B.E., Saul, M.C., Driessen, T.M., and Gammie, S.C. (2013). Development of a versatile enrichment analysis tool reveals associations between the maternal brain and mental health disorders, including autism. BMC neuroscience *14*, 147.

Eisinger, B.E., and Zhao, X. (2018). Identifying molecular mediators of environmentally enhanced neurogenesis. Cell Tissue Res. *371*, 7–21.

Gao, Y., Su, J., Guo, W., Polich, E.D., Magyar, D.P., Xing, Y., Li, H., Smrt, R.D., Chang, Q., and Zhao, X. (2015). Inhibition of miR-15a Promotes BDNF Expression and Rescues Dendritic Maturation Deficits in MeCP2-Deficient Neurons. Stem Cells *33*, 1618–1629.

Gao, Y., Wang, F., Eisinger, B.E., Kelnhofer, L.E., Jobe, E.M., and Zhao, X. (2017). Integrative Single-Cell Transcriptomics Reveals Molecular Networks Defining Neuronal Maturation During Postnatal Neurogenesis. Cereb. Cortex *27*, 2064–2077.

Ge, S., Goh, E.L., Sailor, K.A., Kitabatake, Y., Ming, G.L., and Song, H. (2006). GABA regulates synaptic integration of newly generated neurons in the adult brain. Nature *439*, 589–593.

Ge, S., Pradhan, D.A., Ming, G.L., and Song, H. (2007). GABA sets the tempo for activity-dependent adult neurogenesis. Trends Neurosci. *30*, 1–8.

Giachino, C., Barz, M., Tchorz, J.S., Tome, M., Gassmann, M., Bischofberger, J., Bettler, B., and Taylor, V. (2014). GABA suppresses neurogenesis in the adult hippocampus through GABAB receptors. Development *141*, 83–90.

Gonçalves, J.T., Schafer, S.T., and Gage, F.H. (2016). Adult Neurogenesis in the Hippocampus: From Stem Cells to Behavior. Cell *167*, 897–914.

Gonzalez, J.C., Epps, S.A., Markwardt, S.J., Wadiche, J.I., and Overstreet-Wadiche, L. (2018). Constitutive and Synaptic Activation of GIRK Channels Differentiates Mature and Newborn Dentate Granule Cells. J. Neurosci. *38*, 6513–6526.

Greer, P.L., and Greenberg, M.E. (2008). From synapse to nucleus: calcium-dependent gene transcription in the control of synapse development and function. Neuron *59*, 846–860.

Grégoire, C.A., Bonenfant, D., Le Nguyen, A., Aumont, A., and Fernandes, K.J. (2014). Untangling the influences of voluntary running, environmental complexity, social housing and stress on adult hippocampal neurogenesis. PLoS ONE *9*, e86237.

Grégoire, C.A., Tobin, S., Goldenstein, B.L., Samarut, É., Leclerc, A., Aumont, A., Drapeau, P., Fulton, S., and Fernandes, K.J.L. (2018). RNA-Sequencing Reveals Unique Transcriptional Signatures of Running and Running-Independent Environmental Enrichment in the Adult Mouse Dentate Gyrus. Front. Mol. Neurosci. *11*, 126.

Guo, W., Polich, E.D., Su, J., Gao, Y., Christopher, D.M., Allan, A.M., Wang, M., Wang, F., Wang, G., and Zhao, X. (2015). Fragile X Proteins FMRP and FXR2P Control Synaptic GluA1 Expression and Neuronal Maturation via Distinct Mechanisms. Cell Rep. *11*, 1651–1666.

Habib, N., Li, Y., Heidenreich, M., Swiech, L., Avraham-Davidi, I., Trombetta, J.J., Hession, C., Zhang, F., and Regev, A. (2016). Div-Seq: Single-nucleus RNA-Seq reveals dynamics of rare adult newborn neurons. Science *353*, 925–928.

Hochgerner, H., Zeisel, A., Lönnerberg, P., and Linnarsson, S. (2018). Conserved properties of dentate gyrus neurogenesis across postnatal development revealed by single-cell RNA sequencing. Nat. Neurosci. *21*, 290–299.

Hollinger, S., and Hepler, J.R. (2002). Cellular regulation of RGS proteins: modulators and integrators of G protein signaling. Pharmacol. Rev. *54*, 527–559.

Jobe, E.M., Gao, Y., Eisinger, B.E., Mladucky, J.K., Giuliani, C.C., Kelnhofer, L.E., and Zhao, X. (2017). Methyl-CpG-Binding Protein MBD1 Regulates Neuronal Lineage Commitment through Maintaining Adult Neural Stem Cell Identity. J. Neurosci. *37*, 523–536.

Kempermann, G. (2015). Activity Dependency and Aging in the Regulation of Adult Neurogenesis. Cold Spring Harb. Perspect. Biol. *7*, a018929.

Kempermann, G., Kuhn, H.G., and Gage, F.H. (1997). More hippocampal neurons in adult mice living in an enriched environment. Nature *386*, 493–495.

Kempermann, G., Song, H., and Gage, F.H. (2015). Neurogenesis in the Adult Hippocampus. Cold Spring Harb. Perspect. Biol. *7*, a018812.

Lacar, B., Linker, S.B., Jaeger, B.N., Krishnaswami, S.R., Barron, J.J., Kelder, M.J.E., Parylak, S.L., Paquola, A.C.M., Venepally, P., Novotny, M., et al. (2016). Nuclear RNA-seq of single neurons reveals molecular signatures of activation. Nat. Commun. *7*, 11022.

Langfelder, P., and Horvath, S. (2008). WGCNA: an R package for weighted correlation network analysis. BMC Bioinformatics *9*, 559.

Li, B., and Dewey, C.N. (2011). RSEM: accurate transcript quantification from RNA-Seq data with or without a reference genome. BMC Bioinformatics *12*, 323.

Li, Y., Li, H., Liu, X., Bao, G., Tao, Y., Wu, Z., Xia, P., Wu, C., Li, B., and Ma, L. (2009). Regulation of amygdalar PKA by beta-arrestin-2/phosphodiesterase-4 complex is critical for fear conditioning. Proc. Natl. Acad. Sci. USA *106*, 21918–21923.

Li, Y., Stockton, M.E., Bhuiyan, I., Eisinger, B.E., Gao, Y., Miller, J.L., Bhattacharyya, A., and Zhao, X. (2016). MDM2 inhibition rescues neurogenic and cognitive deficits in a mouse model of fragile X syndrome. Sci. Transl. Med. *8*, 336ra61.

Lin, T.W., Chen, S.J., Huang, T.Y., Chang, C.Y., Chuang, J.I., Wu, F.S., Kuo, Y.M., and Jen, C.J. (2012). Different types of exercise induce differential effects on neuronal adaptations and memory performance. Neurobiol. Learn. Mem. *97*, 140–147.

Lister, R., Mukamel, E.A., Nery, J.R., Urich, M., Puddifoot, C.A., Johnson, N.D., Lucero, J., Huang, Y., Dwork, A.J., Schultz, M.D., et al. (2013). Global epigenomic reconfiguration during mammalian brain development. Science *341*, 1237905.

Livak, K.J., and Schmittgen, T.D. (2001). Analysis of relative gene expression data using real-time quantitative PCR and the 2(-Delta Delta C(T)) Method. Methods *25*, 402–408.

Maity, B., Stewart, A., Yang, J., Loo, L., Sheff, D., Shepherd, A.J., Mohapatra, D.P., and Fisher, R.A. (2012). Regulator of G protein signaling 6 (RGS6) protein ensures coordination of motor movement by modulating GABAB receptor signaling. J. Biol. Chem. *287*, 4972–4981.

Overall, R.W., Paszkowski-Rogacz, M., and Kempermann, G. (2012). The mammalian adult neurogenesis gene ontology (MANGO) provides a structural framework for published information on genes regulating adult hippocampal neurogenesis. PloS one *7*, e48527.

Padgett, C.L., and Slesinger, P.A. (2010). GABAB receptor coupling to G-proteins and ion channels. Adv. Pharmacol. *58*, 123–147.

Piatti, V.C., Davies-Sala, M.G., Espósito, M.S., Mongiat, L.A., Trinchero, M.F., and Schinder, A.F. (2011). The timing for neuronal maturation in the adult hippocampus is modulated by local network activity. J. Neurosci. *31*, 7715–7728.

Pletscher-Frankild, S., Palleja, A., Tsafou, K., Binder, J.X., and Jensen, L.J. (2015). DISEASES: text mining and data integration of disease-gene associations. Methods *74*, 83–89.

Rajan, I., and Cline, H.T. (1998). Glutamate receptor activity is required for normal development of tectal cell dendrites in vivo. J. Neurosci. *18*, 7836–7846.

Ross, E.M., and Wilkie, T.M. (2000). GTPase-activating proteins for heterotrimeric G proteins: regulators of G protein signaling (RGS) and RGS-like proteins. Annu. Rev. Biochem. *69*, 795–827.

Sah, N., Peterson, B.D., Lubejko, S.T., Vivar, C., and van Praag, H. (2017). Running reorganizes the circuitry of one-week-old adult-born hippocampal neurons. Sci. Rep. *7*, 10903.

Sanz, E., Yang, L., Su, T., Morris, D.R., McKnight, G.S., and Amieux, P.S. (2009). Cell-type-specific isolation of ribosome-associated mRNA from complex tissues. Proc. Natl. Acad. Sci. USA *106*, 13939–13944.

Schoenfeld, T.J., McCausland, H.C., Sonti, A.N., and Cameron, H.A. (2016). Anxiolytic Actions of Exercise in Absence of New Neurons. Hippocampus *26*, 1373–1378.

Shen, M., Wang, F., Li, M., Sah, N., Stockton, M.E., Tidei, J.J., Gao, Y., Korabelnikov, T., Kannan, S., Vevea, J.D., et al. (2019). Reduced mitochondrial fusion and Huntingtin levels contribute to impaired dendritic maturation and behavioral deficits in Fmr1-mutant mice. Nat. Neurosci. *22*, 386–400.

Shin, J., Berg, D.A., Zhu, Y., Shin, J.Y., Song, J., Bonaguidi, M.A., Enikolopov, G., Nauen, D.W., Christian, K.M., Ming, G.L., and Song, H. (2015). Single-Cell RNA-Seq with Waterfall Reveals Molecular Cascades underlying Adult Neurogenesis. Cell Stem Cell *17*, 360–372.

Snigdha, S., de Rivera, C., Milgram, N.W., and Cotman, C.W. (2014). Exercise enhances memory consolidation in the aging brain. Front. Aging Neurosci. *6*, 3.

Snyder, J.S., Glover, L.R., Sanzone, K.M., Kamhi, J.F., and Cameron, H.A. (2009). The effects of exercise and stress on the survival and maturation of adult-generated granule cells. Hippocampus *19*, 898–906.

Steib, K., Schäffner, I., Jagasia, R., Ebert, B., and Lie, D.C. (2014). Mitochondria modify exercise-induced development of stem cell-derived neurons in the adult brain. J. Neurosci. *34*, 6624–6633.

Stewart, A., Maity, B., Wunsch, A.M., Meng, F., Wu, Q., Wemmie, J.A., and Fisher, R.A. (2014). Regulator of G-protein signaling 6 (RGS6) promotes anxiety and depression by attenuating serotonin-mediated activation of the 5-HT(1A) receptor-adenylyl cyclase axis. FASEB J. *28*, 1735–1744.

Thompson, A., Boekhoorn, K., Van Dam, A.M., and Lucassen, P.J. (2008). Changes in adult neurogenesis in neurodegenerative diseases: cause or consequence? Genes Brain Behav. *7* (*Suppl 1*), 28–42.

Trapnell, C., Cacchiarelli, D., Grimsby, J., Pokharel, P., Li, S., Morse, M., Lennon, N.J., Livak, K.J., Mikkelsen, T.S., and Rinn, J.L. (2014). The dynamics and regulators of cell fate decisions are revealed by pseudotemporal ordering of single cells. Nat. Biotechnol. *32*, 381–386.

Trinchero, M.F., Buttner, K.A., Sulkes Cuevas, J.N., Temprana, S.G., Fontanet, P.A., Monzón-Salinas, M.C., Ledda, F., Paratcha, G., and Schinder, A.F. (2017). High Plasticity of New Granule Cells in the Aging Hippocampus. Cell Rep. *21*, 1129–1139.

Trinchero, M.F., Herrero, M., Monzon-Salinas, M.C., and Schinder, A.F. (2019). Experience-Dependent Structural Plasticity of Adult-Born Neurons in the Aging Hippocampus. Frontiers in neuroscience *13*, 739.

van Praag, H., Kempermann, G., and Gage, F.H. (1999). Running increases cell proliferation and neurogenesis in the adult mouse dentate gyrus. Nat. Neurosci. *2*, 266–270.

Vivar, C., Potter, M.C., and van Praag, H. (2013). All about running: synaptic plasticity, growth factors and adult hippocampal neurogenesis. Curr. Top. Behav. Neurosci. *15*, 189–210.

Vivar, C., Peterson, B.D., and van Praag, H. (2016). Running rewires the neuronal network of adult-born dentate granule cells. Neuroimage *131*, 29–41.

Winner, B., and Winkler, J. (2015). Adult neurogenesis in neurodegenerative diseases. Cold Spring Harb. Perspect. Biol. *7*, a021287.

Wong, R.O., and Ghosh, A. (2002). Activity-dependent regulation of dendritic growth and patterning. Nat. Rev. Neurosci. *3*, 803–812.

Yamaguchi, M., Saito, H., Suzuki, M., and Mori, K. (2000). Visualization of neurogenesis in the central nervous system using nestin promoter-GFP transgenic mice. Neuroreport *11*, 1991–1996.

Yang, S.M., Alvarez, D.D., and Schinder, A.F. (2015). Reliable Genetic Labeling of Adult-Born Dentate Granule Cells Using Ascl1 CreERT2 and Glast CreERT2 Murine Lines. J. Neurosci. *35*, 15379–15390.

Yun, S., Reynolds, R.P., Masiulis, I., and Eisch, A.J. (2016). Re-evaluating the link between neuropsychiatric disorders and dysregulated adult neurogenesis. Nature medicine *22*, 1239–1247.

Zhao, C., Teng, E.M., Summers, R.G., Jr., Ming, G.L., and Gage, F.H. (2006). Distinct morphological stages of dentate granule neuron maturation in the adult mouse hippocampus. J. Neurosci. *26*, 3–11.

STAR★METHODS

KEY RESOURCES TABLE

REAGENT or RESOURCE	SOURCE	IDENTIFIER
Antibodies		
Rabbit polyclonal anti-RGS6	antibodies-online Inc	Cat#ABIN634403; RRID: AB_2860555
Mouse monoclonal anti-HA.11	Biolegend	Cat#MMS-101R; RRID: AB_291262
Rabbit polyclonal anti-MCM2	Cell Signaling Technology	Cat#4007; RRID: AB_2142134
Goat polyclonal anti-DCX	Santa Cruz Biotechnology	Cat#SC-8066; RRID: AB_2088494
Rabbit polyclonal anti-GFAP	DAKO	Cat#Z0334; RRID: AB_10013382
Rabbit anti-NeuN	Cell Signaling Technology	Cat#24307; RRID: AB_2651140
Rabbit anti-DsRed	Takara	Cat#632496; RRID: AB_10013483
Donkey anti-mouse 488	Thermo Fisher Scientific	Cat#A21202; RRID: AB_141607
Donkey anti-mouse 568	Thermo Fisher Scientific	Cat#A10037; RRID: AB_2534013
Donkey anti-rabbit 488	Thermo Fisher Scientific	Cat#A21206; RRID: AB_2535792
Donkey anti-rabbit 647	Thermo Fisher Scientific	Cat#A31573;RRID: AB_2536183
Donkey anti-goat 568	Thermo Fisher Scientific	Cat#A11057; RRID: AB_2534104
Goat anti-mouse 488	Thermo Fisher Scientific	Cat#A11029; RRID: AB_2534088
Goat anti-rabbit 568	Thermo Fisher Scientific	Cat#A11036; RRID: AB_10563566
Goat anti-rabbit 568	Thermo Fisher Scientific	Cat#A11011; RRID: AB_143157
Bacterial and Virus Strains		
Lentivirus-STOP-RGS6-GFP	This paper	N/A
Lentivirus-STOP-GFP	This paper	N/A
Retrovirus-*shRgs6*-GFP	This paper	N/A
Retrovirus-*shNC*-GFP	(Guo et al., 2015)	https://doi.org/10.1016/j.celrep.2015.05.013; originated from CAG-GFP retroviral vector
Deposited Data		
Source data associated with RiboTag sequencing	This paper	GEO: GSE142678
Experimental Models: Organisms/Strains		
Mouse: C57BL/6J	Jackson Laboratory	RRID:IMSR_JAX:000664
Mouse: Tg(Nestin-cre/ERT2)	Jackson Laboratory	RRID:IMSR_JAX:016261
Mouse: RPL22$^{HA/WT}$	Jackson Laboratory	RRID:IMSR_JAX:029977
Mouse: Ascl1tm1(Cre/ERT2)Jejo/J	Jackson Laboratory	RRID:IMSR_JAX:012882
Mouse: B6;129S6-Gt(ROSA) 26Sortm14(CAG-tdTomato)Hze/J	Jackson Laboratory	RRID:IMSR_JAX:007914
Mouse: Nestin-GFP	(Yamaguchi et al., 2000)	https://doi.org/10.1097/00001756-200006260-00037; Nestin promoter-GFP Transgenic Mice
Oligonucleotides		
Rgs6 Forward: GGATCGCTGATCCAGAAGAG	This study	N/A
Rgs6 Reverse: GGGGATTTTGGAGAGAAAGC	This study	N/A
Pgk1Forward: CTCCGCTTTCATGTAGAGGAAG	This study	N/A
Pgk1Reverse: GACATCTCCTAGTTTGGACAGTG	This study	N/A

(*Continued on next page*)

Continued

REAGENT or RESOURCE	SOURCE	IDENTIFIER
Recombinant DNA		
Retro-CAG-GFP-shRgs6	This study	N/A
Retro-shNC	(Gao et al., 2015)	https://doi.org/10.1016/j.celrep.2015.05.013; Retro-shRNA vector
Retro-CAG-RFP	(Zhao et al., 2006)	https://doi.org/10.1523/JNEUROSCI.3648-05.2006; originated from the CAG-GFP vector
Lenti-GFP-Control	This study	N/A
Lenti-GFP-RGS6	This study	N/A
Software and Algorithms		
Prism	GraphPad	https://www.graphpad.com; RRID:SCR_002798
ImageJ	National Institute of Health	https://imagej.nih.gov/ij/docs/guide/user-guide.pdf
ANYmaze	Stoelting	https://www.stoeltingco.com/anymaze.html
RStudio	Open source software	https://rstudio.com/
WGCNA	(Langfelder and Horvath, 2008)	https://doi.org/10.1186/1471-2105-9-559; open source R package
g:Profiler	BIIT research group	https://biit.cs.ut.ee/gprofiler/gost
Monocle	(Trapnell et al., 2014)	https://doi.org/10.1038/nbt.2859; open source R package

RESOURCE AVAILABILITY

Lead contact

Further information and requests for resources and reagents should be directed to and will be fulfilled by the Lead Contact, Prof. Xinyu Zhao (xinyu.zhao@wisc.edu). Questions for pseudotime and coexpression network analysis should be directed to Dr. Daifeng Wang (daifeng.wang@wisc.edu).

Materials availability

All figures except for Figure 2A were generated from raw data or processed data.

Data and code availability

The accession number for the sequencing data reported in this paper is GEO: GSE142678. The other data generated and/or analyzed during this study are available from the Lead Contact upon reasonable request. Methods for pseudotime and coexpression network analysis are available from Dr. Daifeng Wang (daifeng.wang@wisc.edu)

EXPERIMENTAL MODEL AND SUBJECT DETAILS

Mice and animal husbandry

We performed all procedures involving live mice in accordance with the NIH Guide for the Care and Use of Laboratory Animals and the protocols approved by the University of Wisconsin-Madison and the University of Alabama at Birmingham Animal Care and Use Committee. We generated the inducible conditional ribosome tagging female mice (Tg(Nestin-cre/ERT2)::RPL22HA/WT, simplified as Nes-CreERT2::RiboTag) by crossing transgenic driver Tg(Nes-cre/ERT2) mice (Jackson Laboratory Stock No:016261) (Lagace et al., 2007) with RPL22HA/WT mice (Jackson Laboratory Stock No:029977) (Sanz et al., 2009). Nestin-GFP male mice were the same mouse line published previously (Jobe et al., 2017). Mice were kept in 12 h light/12 dark cycle housing. Both the Tg(Nes-Cre/ERT2) and RPL22HA/WT mice were C57BL/6J genetic background. To induce recombination, mice (9–11 weeks old) received Tamoxifen (Sigma-Aldrich) daily for 5 days (160 mg kg–1 i.p., 40 mg ml–1 in 10% ethanol mixed with sunflower oil, Sigma-Aldrich). Running mice were individually housed in regular mouse cages that contain one running wheel with wireless monitor per cage (Med Associates inc). Sedentary mice were housed in identical cages as running mice except that the wheels were glued (blocked) and without wireless monitor (Med Associates, inc). To record from newly generated adult born neurons, we used Ascl1CreERT2 (Ascl1tm1(Cre/ERT2)Jejo/J) male and female mice, obtained from the Jackson Laboratory (Stock No:012882) crossed with

CAGfloxStop-tdTomato (Ai14) (B6;129S6-Gt(ROSA)26Sortm14(CAG-tdTomato)Hze/J) conditional reporter line (Jackson Laboratory Stock No:007914). Tamoxifen was delivered as described above. Functional and locked running wheels were attached to standard cages (Kaytee brand). The mice were kept in 12 h light/12 dark cycle housing.

METHOD DETAILS

Tissue preparation, immunohistochemistry and confocal imaging

Brain tissue processing and histological analysis of mouse brains were performed as described in our publications (Gao et al., 2015, 2017). For *in vivo* cell proliferation analyses using BrdU labeling, mice were given two intraperitoneal injections of BrdU (100 mg/kg) 24 h before perfusion. At 11, 18 or 27 days after wheel running, mice were euthanized by intraperitoneal injection of sodium pentobarbital and then transcardially perfused with saline followed by 4% PFA. Brains were dissected out, post-fixed overnight in 4% PFA, and then equilibrated in 30% sucrose. Forty-μm brain sections were generated using a sliding microtone and stored in a –20°C freezer as floating sections in 96-well plates filled with cryoprotectant solution (glycerol, ethylene glycol, and 0.1M phosphate buffer, pH 7.4, 1:1:2 by volume). Immunohistology was performed as published previously (Gao et al., 2015, 2017). The tissue sections were pre-blocked with TBS++ (TBS containing 3% goat or donkey serum and 0.2% Triton X-100) for 1 h at room temperature, followed by incubation with primary antibodies diluted in TBS++ overnight in 4°C. After washing 3 times, secondary antibodies were incubated 1 h at room temperature. All sections were counterstained with a nuclear counter stain, DAPI (4', 6-diamidine-2′-phenylindole dihydrochloride, 1:2000, Roche Applied Science, Indianapolis, IN). For RGS6 staining, before blocking, there was an antigen retrieval treatment with 10 mM sodium citrate (pH 9) for 30 min at 80°C. For BrdU staining, we performed immunohistological analysis on 1-in-6 serial floating brain sections (240 mm apart).

The primary antibodies used were: Rabbit anti-RGS6 (1:200, antibodies-online Inc., #ABIN634403, Limerick, PA, USA), Mouse anti-HA.11 (1:1000, Covance (now Biolegend), # MMS-101R, Princeton, NJ, USA), Rabbit anti-MCM2 (1:1000, Cell Signaling Technology, Inc., #4007, Danvers, MA, USA), Goat anti-DCX (1:500, Santa Cruz Biotechnology, Inc., # SC-8066, Dallas, TX, USA), Rabbit anti-GFAP (1:2000, DAKO, #Z0334, Carpinteria, CA, USA), Rabbit anti-NeuN (1:3000, Cell Signaling Technology, Inc., #4007, Danvers, MA, USA), Rabbit anti-Phospho-CREB(Ser133) (1:800, Cell Signaling Technology, Inc., #9198S, Danvers, MA, USA). Fluorescent secondary antibodies used by 1:1000 dilution: Donkey anti-mouse 488 (A21202, Invitrogen), Donkey anti-mouse 568 (A10037, Invitrogen), Donkey anti-rabbit 488 (A21206, Invitrogen), Donkey anti-rabbit 647 (A31573, Invitrogen), Donkey anti-goat 568 (A11057, Invitrogen), Goat anti-mouse 488 (A11029, Invitrogen), Goat anti-rabbit 568 (A11036, Invitrogen), After staining, sections were mounted and maintained at 4oC in the dark until analysis. Z stack confocal images were taken using Nikon A1 confocal microscope. The Z stack images were analyzed using a Zeiss Apotome microscope equipped by StereoInvestigator and Microlucida software (MBF Biosciences,Inc.)

Plasmids

Retro-CAG-GFP-*shRgs6* was cloned using Retro-shNC (Guo et al., 2015) as the backbone. Briefly, U6-shNC cassette was cloned into the backbone through HpaI/ClaI restriction sites. Retro-Cre were generated by replacing red fluorescent protein (RFP) coding sequence in the Retro-CAG-RFP (Zhao et al., 2006) with Cre coding sequence. Lenti-GFP-Control and Lenti-GFP-RGS6 were generated using lenti-CMV-GFP vector as a backbone and the CMV-GFP cassette were replaced with CAG-LoxP-STOP-LoxP-GFP and CAG-LoxP-STOP-LoxP-GFP-P2A-RGS6 correspondently. The Rgs6 shRNA sequences are: shRgs6-1: 5'- CAAGTGAAGATTGACCGGAAA-'3; shRgs6-2: 5'- CGGCGTTTGAAGAATCCACAA -'3; shRgs6-3: 5'- GCTATGAGATAACCAGTCAAA -'3.

Production of lentivirus and retrovirus

Lentivirus and retrovirus production were performed using previous protocol (Gao et al., 2015, 2017) with modification. Briefly, lentiviral DNA was co-transfected with packaging plasmids pMDL, REV and pCMV-Vsvg into HEK293T cells using PEI method. Retroviral DNA was co-transfected with packaging plasmids pCMV-gag-pol and pCMV-Vsvg into HEK293T cells using PEI method. The viral transfer vector DNA and packaging plasmid DNA were transfected into 5X15 cm dishes of cultured HEK293T cells using PEI. The medium containing lentivirus was collected at 36, 60 and 84 h post-transfection, pooled, filtered through a 0.2-μm filter, and concentrated using an ultracentrifuge at 19,000 rpm for 2 h at 4°C using a SW32Ti rotor (Beckman). The virus was washed once and then resuspended in 100 μl PBS. We routinely obtained $1X10^9$ infectious viral particles /ml for lentivirus and $1X10^8$ infectious viral particles /ml for retrovirus.

In vivo retroviral grafting and morphological analysis of targeted neurons

In vivo virus grafting was performed as described (Gao et al., 2015). Briefly, 7-week-old male mice were anesthetized with isofluorane and placed in a stereotactic instrument (DAVID KOPF Instruments, Tujunga, CA). Microinjections were performed using custom-made injection 33-gauge needles (Hamilton, #776206, Reno, NV, USA) connected to a 10 μL syringe (Hamilton, #87930). Virus (1.25 μl with titer greater than $1X10^8$/ml) was mixed and then stereotaxically injected into the dentate gyrus using the following

coordinates relative to bregma, caudal: +2.0 mm; lateral: +/−1.6 mm; ventral: −1.9 mm. 17, 19 or 21 days post viral grafting, mice were perfused for different analysis. Mice were deeply anesthetized with pentobarbital and perfused with saline followed by 4% PFA. Morphological analyses of retroviral labeled new neurons were performed as described (Gao et al., 2015). Two hundred micrometer-thick floating brain sections containing eGFP were selected. For dendritic branching analysis, GFP-positive cells were imaged on an A1 confocal microscope. The dendrites and the cell body of single expression of GFP neurons were analyzed by Neurolucida software (Micro-BrightField, Burlington, Vermont, https://www.mbfbioscience.com/). At least 30 neurons per group were traced.

In vivo cell quantification

Quantification of BrdU+ cells in the adult DG was performed using an AxioImagerZ2 ApoTome microscope (Zeiss) equipped with motorized stage and operated by StereoInvestigator software (MBF Biosciences, Inc). The cell number was quantified using design-based stereology with the optical fractionator function of StereoInvestigator software (MBF Biosciences, Inc), as described (Li et al., 2016; Shen et al., 2019). Briefly, 1 in 6 serial 40 μm brain sections starting at beginning of hippocampus (relative to bregma, −1.5 mm) to the end of hippocampus (relative to bregma, −3.5 mm) were selected for staining using an anti-BrdU antibody as described above. The thickness of the mounted sections were measured (around 30 um) and guard zones of 3 μm were set for each surface of the section. The contour of the DG was drawn with one cell body extra space along the hilar surface of the DG. The counting frame was set at 200.0 μm width (X) and 200.0 μm height (Y). The number of sampling sites were around 350 and the section evaluation interval was 6. The estimated CE (Cruz-Orive/Geiser) < 0.1. Approximately 10-100 cells were counted in each DG (one side). The total number of cells were calculated using StereoInvestigator using preset algorithm. The volume of analyzed region for each animal was obtained. The percentage of HA+ cells that were colabeled with other cell markers was analyzed as described previously (Li et al., 2016; Shen et al., 2019). Briefly, the z stack images about 500-1200 BrdU+ cells were obtained using an AxioImagerZ2 ApoTome confocal microscope (Zeiss).

Immunofluorescent intensity quantification

The signal intensity of RGS6 in HA+ cells in the DG of Tamoxifen injected Nes-CreERT2;RiboTag mice was quantified using ImageJ software. The z stack images were acquired using Nikon A1 confocal microscope at 20X magnification with 2 μm interval. A line was drawn through the soma without the cell nuclear of each HA+ cell and the intensity of RGS6 was measured using ImageJ. The background area was selected and measured with ImageJ as well. The RGS6 intensity values were calculated as: (RGS6 Area) * (RGS6 mean intensity – Background mean intensity). In total, 5 running mice (115 cells) and 6 sedentary mice (90 cells) were used for this quantification.

RiboTag-Seq and identification of differentially expressed genes (DEGs)

Dentate gyri were dissected from 2-4 Nes-HA mice from either running or sedentary conditions, pooled, and immediately homogenized in 1ml of homogenization buffer (50mM Tris [pH 7.4], 100mM KCl, 12mM MgCl2, 1% IGEPAL, 1mM DTT, 1x RNase inhibitor, 100 μg/mL Cycloheximide, 1mg/mL Heparin) with 1X complete protease inhibitors (Roche). Nuclei and debris were pelleted at 10,000 X g for 10 min. An aliquot (20 μl) of lysate input was saved for extraction of input (IN) RNA. 3-6 μL monoclonal antibody against HA Tag (Covance catalog# MMS-101R) was incubated with supernatant at 4°C for 6 hr and before adding Dynabeads (ThermoFisher). The antibody/Dynabeads conjugation was rotated at 4°C overnight and washed with high salt buffer (50mM Tris [pH 7.4], 300mM KCl, 12mM MgCl2, 1% IGEPAL, 1mM DTT, 100 μg/mL Cycloheximide) to remove unbound proteins and RNA. Finally, Trizol was added to the beads and the supernatant was saved for RNA isolation. RNA from the RiboTag IP was isolated using the Direct-zol RNA MicroPrep Kit (Zymo Research Corporation. Irvine, CA, USA). Quality, size, and concentration of the isolated RNA were analyzed using Bioanalyser 2100 (RNA Pico Kit, Agilent). The libraries were then made using SMARTer® Stranded Total RNA-Seq Kit v2 (Takara Bio USA, Inc. Mountain View, CA) according to the user manual. The constructed libraries were analyzed with Qubit (ThermoFisher Scientific, Waltham, MA) and Bioanalyser 2100 (RNA Pico Kit, Agilent). Cluster generation and high-throughput sequencing were performed on a HiSeq 2500 (Illumina), using the single-end 100 bp protocol. RSEM was used to align read pairs to the mm10 transcriptome and estimate gene expression levels (Li and Dewey, 2011). Differentially expressed genes (DEGs) were successfully identified in running mice using embedded EBseq in RSEM with a cutoff of 0.05 of "PPEE" (posterior probability estimated by EBseq that a gene/transcript is equally expressed). The next generation sequencing data have been submitted to GEO (GSE142678).

Single Cell trajectory by pseudotime analysis

We performed the pseudo-timing analysis for our IP dataset and the Div-Seq single cell dataset for neuronal development (270 cells) covering the stages of 1-2, 3-4, 5-6, 6-7, 7-14 day (Habib et al., 2016). In particular, we input gene expression data (TPM values) of these datasets to Monocle (Trapnell et al., 2014) for revealing the pseudo timing. The differentially expressed genes (n = 460) between running and sedentary samples at Day-18 were used to construct the developmental trajectories (Figure 2A), representing pseudotiming ordering between Div-Seq cells and our six IP samples (running and sedentary Day- 11, 18, 27).

Gene co-expression network and module analysis

We constructed the gene co-expression networks by connecting all possible gene pairs by edges with edge weights being the Pearson correlations of their time-series gene expression profiles across Day-11, Day-18 and Day-27 for running and sedentary datasets.

The gene co-expression network was further clustered by WGCNA (weighted correlation network analysis), R package (Langfelder and Horvath, 2008) into the gene co-expression modules (minimum module size = 100 genes, scale-free fitting beta > 0.8). The eigengenes of modules were calculated and provided by WGCNA as well. An eigengene is a vector with its elements representing the expression levels across time points, representing the most likely temporal gene expression changes across time points (temporal dynamic pattern) of its co-expression module.

Enrichment analysis

Enrichment analyses including GO, KEGG and REACTOME for differentially expressed genes or gene co-expression modules were performed in ''g:GOST'' fuctional profiling using g: Profiler (https://biit.cs.ut.ee/gprofiler/gost). Genes linked to adult hippocampal neurogenesis were downloaded from the Mammalian Adult Neurogenesis Gene Ontology (MANGO) database (http://mango.adult-neurogenesis.de/documents/annotations?show=20&expression=true) (Overall et al., 2012). Genes that are demethylated during development of the mammalian brain were provided by Lister et al. (Lister et al., 2013) Disease-linked genes were curated from Phenocarta (https://pavlidislab.github.io/Gemma/phenocarta.html), the DISEASES database (https://diseases.jensenlab.org/Search) (Pletscher-Frankild et al., 2015), and AutDB (http://autism.mindspec.org/autdb/Welcome.do) (Basu et al., 2009). Overrepresentation of gene sets was statistically assessed within identified gene clusters against the transcriptome background in R using the Modular Single-set Enrichment Test (Eisinger et al., 2013).

RNA isolation, cDNA synthesis and qPCR

RNA was isolated from TRIzol samples using the TRIzol Reagent following the manufacturer's instructions. Reverse transcription and Real-time PCR was performed using standard methods as described (Gao et al., 2015). The first-strand complementary DNA (cDNA) was generated by reverse transcription with Random 6 mers primer (Takara Bio USA, Inc. Mountain View, CA). To quantify the mRNA expression using real-time PCR, aliquots of first-stranded cDNA were amplified with gene-specific primers and Power SYBR Green PCR Master Mix (Bio-Rad) using a StepOne Real-Time PCR System (Applied Biosystems). The PCR reactions contained cDNA, Universal Master Mix (Applied Biosystems), and 10 mM of forward and reverse primers in a final reaction volume of 20 ml. The mRNA expression of different samples was calculated using $2^{\Delta\Delta Ct}$ method (Livak and Schmittgen, 2001).

Electrophysiology

Three weeks after virus injection, mice were euthanized with CO_2 and decapitated, followed by quick transfer of brain into ice-cold dissection solution comprising (mM) 93 NMDG, 93 HCl, 2.5 KCl, 1.2 NaH2PO4, 30 NaHCO3, 20 HEPES, 25 glucose, 5 sodium ascorbate, 2 Thiourea, 3 sodium pyruvate, 10 MgSO4, 0.5 CaCl2. Coronal slices (400 μm thick) were obtained and transferred to artificial cerebrospinal fluid (ACSF) containing (mm): 124 NaCl, 2.5 KCl, 2.5 CaCl2, 1.2 MgCl2, 1.25 NaH2PO4, 26 NaHCO3, and 15 glucose (equilibrated with 95% O2 and 5% CO2; pH 7.4). Slices were incubated at 34 °C for 10 min and stored at room temperature for 1 hour for recovery. Then slices were transferred to a submerged recording chamber (flow rate 2-2.5 ml/min at room temperature). For recording miniature excitatory postsynaptic currents (mEPSCs), pipettes were filled with (in mM): 140 K-gluconate, 7.5 KCl, 10 HEPES-K, 0.5 EGTA-K, 4 Mg-ATP and Li-GTP (pH 7.2). mEPSCs were recorded in the presence of 1 mM tetrodotoxin (TTX). Adult born neurons were identified by expression of GFP under epifluorescence using differential interference contrast video microscopy and recorded in voltage clamp mode (−70 mV). Whole-cell patch-clamp recordings were filtered at 2 kHz and digitalized at 10 kHz using Multiclamp 700B, Digidata 1440 A and pClamp 10.4 Software (Molecular Devices). Series resistance was typically within 10–30 MΩ. Miniature EPSC events were analyzed using Python. Threshold was typically kept at −5 pA and adjusted with respect to the baseline noise. Artifacts were screened through visual inspection and overlapping events (event frequency of ≥ 100 Hz) were discarded. Raw current traces of 300 s were analyzed for peak amplitude and frequency which were averaged for each cell and used for further statistical analysis.

For recording Ca^{2+} currents, Ascl1-CreERT2::Ai14 or virus-injected mice were anesthetized with 2,2,2-tribromoethanol (Avertin; Sigma-Aldrich), and perfused intracardially with ice-cold modified ACSF containing the following (in mM): 110 choline chloride, 25 D-glucose, 7 $MgCl_2$, 2.5 KCl, 1.25 Na_2PO_4, 0.5 $CaCl_2$, 1.3 Na-ascorbate, 3 Na-pyruvate, and 25 $NaHCO_3$, bubbled with 95% O_2/5% CO2. Brains were removed and horizontal slices (300 μm) from both hemispheres were cut using a vibratome (VT1200S, Leica Instruments) and transferred to a chamber containing recording ACSF (in mM) as follows: 125 NaCl, 2.5 KCl, 1.25 Na_2PO_4, 2 $CaCl_2$, 1 $MgCl_2$, 25 $NaHCO_3$, and 25 D-glucose bubbled with 95% O2/5% CO_2. Slices were incubated at 37°C for 30 min and then stored at room temperature for at least 30 min before mounted on a BX51WI Olympus microscope and superfused with ACSF solution at 30°C. Immature neurons were visually identified in the granule cell layer by fluorescence (TxRed or GFP-A filter sets, Leica) using custom Dodt gradient contrast videomicroscopy. Whole-cell calcium currents were recorded with fire-polished borosilicate glass electrodes (outer diameter, 1.5 mm, inner diameter, 0.86 mm; Sutter Instrument) with resistance of 5–7 MΩ when filled with the following intracellular solution (in mM): 122 CsMeSO3, 9 HEPES, 1.8 MgCl2, 4 Mg-ATP, 0.3 Na-GTP, 14 phosphocreatine, 0.45 EGTA, pH 7.3. Pipettes were mounted on the headstage (CV-7B) of a Multiclamp 700A amplifier (Molecular Devices) with cancellation of pipette capacitive transients. Currents were filtered at 2 kHz and sampled at 10 kHz. Calcium currents were isolated using NBQX (10 μM), R-CPP (5 μM), SR9553 (10 μM) and

TTX (1 μM) with extracellular calcium in the ACSF exchanged for 2 mM $BaCl_2$. The holding potential was set at −70 mV and 200 ms voltage steps to 0 mV were applied to evoke calcium currents every 20 s. Capacitance and leak currents were subtracted using P/4 leak subtraction. Currents were analyzed with Axograph X (Axograph Scientific) or Clampfit (Molecular Devices). Peak amplitude was measured from an average of 5-10 currents in each condition and normalized to capacitance that was measured from a 10 mV voltage step. Recordings and analysis were performed blinded to condition. Drugs and chemicals were obtained from Sigma-Aldrich, Tocris Bioscience, or Ascent Scientific. Two-tailed paired or unpaired t tests were used with significance at $p < 0.05$ (GraphPad Software). TdTomato fluorescence in fixed sections (50 μm) from Ascl1CreERT2/Ai14 mice was amplified with rabbit anti-DsRed polyclonal antibody (1:800, #632496, Takara) and goat anti-rabbit Alexa Fluor 568 (1:400, A-11011, Invitrogen). Sections were imaged with a water-immersion objective on a confocal microscope (10x, Olympus FV1200, z steps of 0.5 μm).

Behavioral analysis

Viral injected mice were subjected to either freely running wheel (Run) or locked wheels (sedentary controls) for 27 days before behavioral testing. All mice were subjected to open-field activity chamber test for assessing their general health and activity levels, both before and after the behavioral tests described below. The mice were always subjected to elevated plus maze first, then novel location text, and finally fear condition test.

Elevated plus-maze

Elevated plus-maze test was performed using the procedure described (Allan et al., 2008). Mice were placed in the center square (6X 6 cm) of a Plexiglas maze shaped in a cross that was elevated two feet above the ground and was located in a moderately lit, sound-attenuated room. The supports for the maze were made of clear Plexiglas and were positioned in the middle of the arms, so the mouse was unable to detect them. The maze had two open arms (30X6 cm each) that were made of clear Plexiglas floor with no wall. The closed arms were covered with black contact paper and had 6 cm high walls covered with black contact paper. An observer blind to genotype monitored behavior for 10 min. The time spent in the open arms and closed arms and the numbers of entries into each arm were recorded. The data were analyzed using one way ANOVA.

Novel location test

This test measures spatial memory through an evaluation of the ability of mice to recognize the new location of a familiar object with respect to spatial cues. The procedures of this test was performed as previously described (Shen et al., 2019). Briefly, mice were handled for approximately 5min per day for a maximum of 5 days prior to the experiment. All procedures were conducted during the light cycle of the animal between 9 a.m. and 6 p.m. Before the trial session, mice were brought into testing room and were allowed to acclimate for at least 30min. Testing consisted of five 6-min trials, with a 3-min intertrial interval between each trial. During the intertrial interval, the mouse was placed in a holding cage, which remained inside the testing room. In the first trial (pre-exposure), each mouse was placed individually into the center of the otherwise empty open arena (38.5 cm long × 38.5 cm wide, and 25.5 cm high walls) for 6min. For the next three trials (sample trials 1–3), two identical objects were placed equidistantly from the arena wall in the corners against the wall with the colored decal. Objects were taped to the floor of the arena. Then, each mouse was placed individually into the center of the arena and allowed to explore for 6min. At the end of the trial, the mouse was removed and returned to the home cages for 3min. In the last trial (test), one of the objects was moved to a novel location, and the mouse was allowed to explore the objects for 6 min, and the total time spent exploring each object was measured. During the test phase, exploration time was defined as any investigative behavior (that is, head orientation, climbing on, sniffing occurring within < 1.0 cm) or other motivated direct contact occurring with each object. To control for possible odor cues, objects were cleaned with 70% ethanol solution at the end of each trial and the floor of the arena wiped down to eliminate possible scent/trail markers. During the test phase, two objects were wiped down prior to testing so that the objects would all have the same odor. The discrimination index was calculated as the percentage of time spent investigating the object in the new location minus the percentage of time spent investigating the object in the old location: discrimination index = (novel location exploration time/total exploration time × 100) – (old location exploration time/total exploration time × 100). A higher discrimination index is considered to reflect greater memory retention for the novel location object. All experiments were videotaped and scored by scientists who were blinded to experimental conditions to ensure accuracy.

Fear conditioning

These tests were performed based on published method with modification (Li et al., 2009). Apparatus: Animals were placed into a Coulbourn Habitest fear conditioning system equipped with a stainless-steel grid floor for administration of a foot shock. Training: After 2.5 min of habituation in the conditioning apparatus, a 2 s electric foot shock of 0.7mA was presented. Mice were left in the conditioning apparatus for 30 more seconds, then were returned to their home cages. Testing: At 24 h following training mice were tested for context freezing. For the context freezing, mice were placed into the conditioning context for 300 s and were observed for freezing behavior throughout the context testing period. Behavior was analyzed in a blinded fashion with regard to genotype and treatment. All training was videotaped for subsequent viewing, re-scoring and documentation. The trace conditioning apparatus was cleaned between each mouse with 70% isopropylalcohol.

QUANTIFICATION AND STATISTICAL ANALYSIS

Statistical analysis

Statistical analysis was performed using ANOVA and Student's t test, unless specified, with the aid of SPSS version 22 and GraphPad software. Two tailed and unpaired t test was used to compare two conditions. Two-way ANOVA with Tukey's post hoc analysis was used for analyzing multiple groups. One-Way ANOVA with Bonferroni post hoc test used for comparison among for *in vivo* dendritic analysis of different genotypes (GraphPad software 6). Scholl analysis was carried out using multivariate analysis of variance (MANOVA) using SPSS statistical software. All data were shown as mean with standard error of mean (mean ± SEM). Probabilities of $p < 0.05$ were considered as significant.

Update

Cell Reports

Volume 32, Issue 8, 25 August 2020, Page

DOI: https://doi.org/10.1016/j.celrep.2020.108114

Cell Reports

CellPress
OPEN ACCESS

Correction

RGS6 Mediates Effects of Voluntary Running on Adult Hippocampal Neurogenesis

Yu Gao, Minjie Shen, Jose Carlos Gonzalez, Qiping Dong, Sudharsan Kannan, Johnson T. Hoang, Brian E. Eisinger, Jyotsna Pandey, Sahar Javadi, Qiang Chang, Daifeng Wang, Linda Overstreet-Wadiche, and Xinyu Zhao*
*Correspondence: xinyu.zhao@wisc.edu
https://doi.org/10.1016/j.celrep.2020.108114

(Cell Reports *32*, 107997-1–107997-15, e1–e7; August 4, 2020)

In the originally published version of this article, there were multiple incorrect citations. The following citations were originally omitted but have now been included: Basu et al. (2009); Bracko et al. (2012); Brandt et al. (2003); Eisinger et al. (2013); Ge et al. (2006); Lister et al. (2013); Overall et al. (2012); Pletscher-Frankild et al. (2015); Trinchero et al. (2019); and Yun et al. (2016). Additionally, the following references were originally included but have now been deleted: Langfelder et al. (2007); Raudvere et al. (2019); Gould et al. (1999); and Zhao et al. (2008). The citations and references have now been corrected online.

The authors regret this error.